THE JOURNAL OF BIOLOGICAL CHEMISTRY VOL. 291, NO. 29, pp. 15029–15045, July 15, 2016

Urokinase-type Plasminogen Activator (uPA) Promotes Angiogenesis by Attenuating Proline-rich Homeodomain Protein (PRH) Transcription Factor Activity and De-repressing Vascular Endothelial Growth Factor (VEGF) Receptor Expression*[S]

Received for publication, July 13, 2015, and in revised form, May 3, 2016 Published, JBC Papers in Press, May 4, 2016, DOI 10.1074/jbc.M115.678490

Victoria Stepanova[‡1,2], Padma-Sheela Jayaraman[§1], Sergei V. Zaitsev[¶1], Tatiana Lebedeva[‡], Khalil Bdeir[‡], Rachael Kershaw[§], Kelci R. Holman[‖], Yelena V. Parfyonova[‡‡], Ekaterina V. Semina[**‡‡], Irina B. Beloglazova[**], Vsevolod A. Tkachuk[**‡‡], and Douglas B. Cines[‡]**

*From the Departments of [‡]Pathology and Laboratory Medicine and [¶]Pharmacology, Perelman School of Medicine, University of Pennsylvania, Philadelphia, Pennsylvania 19104, [§]School of Immunity and Infection, College of Medical and Dental Sciences, University of Birmingham, Edgbaston, Birmingham B152TT, United Kingdom, **Russian Cardiology Research Center, Moscow 121552, Russia, [‡‡]School (Faculty) of Fundamental Medicine, Lomonosov Moscow State University, Moscow, 117192, Russia, and [‖]College of Arts and Sciences, Drexel University, Philadelphia, Pennsylvania 19104*

Urokinase-type plasminogen activator (uPA) regulates angiogenesis and vascular permeability through proteolytic degradation of extracellular matrix and intracellular signaling initiated upon its binding to uPAR/CD87 and other cell surface receptors. Here, we describe an additional mechanism by which uPA regulates angiogenesis. *Ex vivo* VEGF-induced vascular sprouting from Matrigel-embedded aortic rings isolated from uPA knock-out ($uPA^{-/-}$) mice was impaired compared with vessels emanating from wild-type mice. Endothelial cells isolated from $uPA^{-/-}$ mice show less proliferation and migration in response to VEGF than their wild type counterparts or $uPA^{-/-}$ endothelial cells in which expression of wild type uPA had been restored. We reported previously that uPA is transported from cell surface receptors to nuclei through a mechanism that requires its kringle domain. Intranuclear uPA modulates gene transcription by binding to a subset of transcription factors. Here we report that wild type single-chain uPA, but not uPA variants incapable of nuclear transport, increases the expression of cell surface VEGF receptor 1 (VEGFR1) and VEGF receptor 2 (VEGFR2) by translocating to the nuclei of ECs. Intranuclear single-chain uPA binds directly to and interferes with the function of the transcription factor hematopoietically expressed homeodomain protein or proline-rich homeodomain protein (HHEX/PRH), which thereby lose their physiologic capacity to repress the activity of vehgr1 and vegfr2 gene promoters. These studies identify uPA-dependent de-repression of vegfr1 and vegfr2 gene transcription through binding to HHEX/PRH as a novel mechanism by which uPA mediates the pro-angiogenic effects of VEGF and identifies a potential new target for control of pathologic angiogenesis.

In the healthy adult blood vessels show little or no growth or extension except during the ovarian cycle and during placental development, and there is minimal physiologic turnover of vascular endothelial cells (1). Angiogenesis, the process by which new blood vessels develop from pre-existing vasculature, is activated by diverse pathophysiological stimuli, such as hypoxia, inflammation, or wounding, and the vessels return to the quiescent state once these stimuli are removed or wound closure has been attained (1, 2). These complex processes of physiological and adaptive angiogenesis require a finely tuned balance between integrins, angiopoietins, chemokines, junctional molecules, oxygen sensors, matrix components, endogenous inhibitors, and many other factors (3).

However, there are prevalent and important settings (malignancy, inflammation, diabetic retinopathies, and development of atherosclerotic plaques, among others) in which pro-angiogenic stimuli predominate, resulting in what has been referred to as the "angiogenic switch" (4, 5). Persistent excessive neoangiogenesis may be deleterious to the host, *e.g.* enhancing tumor growth or proliferation of "leaky" retinal vessels subject to rupture. A more thorough understanding of the process underlying the angiogenic switch that are not shared by normal vessels might identify steps in the process that could be subject to therapeutic intervention aimed at suppressing excessive neoangiogenesis or safely inducing therapeutic angiogenesis.

Early in angiogenesis, endothelial cells divide, migrate, degrade, and invade abluminal basement membrane forming and stable vascular tubular structures (2). Urokinase-type plas-

* This work was supported by National Institutes of Health Grants HL116916 (to D. B. C.), CA141228 (to V. S.), and R21-AI-102177 (to K. B.). This work was also supported by Russian Science Foundation Grant 14-24-00086 (to V. A. T.) and by Russian Foundation for Basic Research Grants 13-04-02014-a (to Y. V. P.) and 16-04-01699 (to I. B. B.). The authors declare that they have no conflicts of interest with the contents of this article. The content is solely the responsibility of the authors and does not necessarily represent the official views of the National Institutes of Health.

[S] This article contains supplemental Movies 1 and 2.

[1] These authors contributed equally to this work.

[2] To whom correspondence should be addressed: 512 Stellar Chance Bldg., 422 Curie Blvd., Philadelphia, PA, 19104. Tel.: 215-662-7757; Fax: 215-573-2012; E-mail: vstepano@mail.med.upenn.edu.

minogen activator (uPA),[3] its high affinity receptor (uPAR; CD87), and its inhibitor plasminogen activator inhibitor 1 (PAI-1) have been implicated in each of these steps (6–8). Resting endothelial cells express low levels of uPA and uPAR, whereas their expression is strongly up-regulated during angiogenesis (9, 10). uPA promotes pro-angiogenic signaling upon binding to several interacting surface receptors, including uPAR (CD87), LDL receptor-related protein receptor (LRP/α2MR), and specific integrins (11–17). uPA also enzymatically converts plasminogen into the broadly acting serine protease plasmin (18, 19) that degrades matrix proteins and activates several matrix metalloproteinases (20–23). uPAR-bound uPA is typically localized on the leading edge of migrating endothelial and other cells (24–26) where it not only helps to maintain focused degradation of extracellular matrix but also to liberate matrix-bound pro-angiogenic growth factors, such as VEGF (27–29) and basic FGF (bFGF/FGF-2) (30, 31) via plasmin-dependent proteolysis. uPA also directly activates VEGF-A189 through proteolytic cleavage independent of plasmin (32).

uPA has also been implicated in the process through which VEGF stimulates endothelial cell proliferation and forms new blood vessels. For example, exogenous VEGF does not induce angiogenesis when injected into infarcted myocardium in uPA knock-out mice (uPA$^{-/-}$ mice) (33). VEGF-induced endothelial permeability also depends on uPA and uPAR (34). Endothelial cells derived from uPA$^{-/-}$ mice do not overexpress the X-linked inhibitor of apoptosis (XIAP), which maintains endothelial survival in response to VEGF unless uPA is restored (35). We have also reported that uPA enhances endothelial permeability through intracellular signaling pathways shared with VEGF (36). However, the possibility that uPA contributes to VEGF-induced signaling through pathways unrelated to proteolysis and receptor-mediated intracellular signaling has not been explored.

We recently reported that single-chain uPA (scuPA) translocates to the nuclei of proliferating cells (37) where it regulates transcription factor HOXA5 (38), which is involved in endothelial cell proliferation and repair (39, 40). In this manuscript we provide insight into a novel mechanism through which uPA mediates the pro-angiogenic effects of VEGF. We show that scuPA translocates to the nuclei of endothelial cells where it binds to the homeobox transcription factor HHEX, a repressor of *vegfr1* and *vegfr2* gene promoters, and in doing so interferes with their function and thereby induces VEGF receptor expression. These findings delineate a novel mechanism that contributes to the regulation of endothelial proliferation and a potential new approach toward control of aberrant angiogenesis.

Experimental Procedures

Vector Constructs

HHEX-FLAG/pcDNA3.1 Constructs—A vector encoding ΔNLS-mouse nucleolin, described previously (37), was used to amplify a pcDNA3.1-FLAG fragment to retain FLAG within the pcDNA3.1 vector sequence and introduce Xho1 restriction site at the 5′ end and EcoR1 site at the 3′ end using the primers: forward 5′-TGCTGGACGCTCGAGCGACTACAAAGACG-ATGACGAT-3′ and reverse 5′-TGCATAGTGAATTC-CAGCACACTGGCGGCCGT-3′.

Full-length HHEX was amplified using the primers P1 (forward) and P2(reverse) to introduce EcoRI and XhoI restriction sites, respectively (P1, 5′-TGCTGGAATTCACTATGCAGT-ACCCGCACCCCGGGCC-3′; P2, 5′-GTAGTCGCTCGAGC-GTCCAGCATTAAAATAGC-3′), and cDNA encoding human HHEX (Thermo/Open Biosystems) was used to amplify HHEX. The fragment was restricted with EcoR1 and Xho1 and ligated with the pcDNA3.1-FLAG fragment to obtain the vector encoding HHEX which possesses FLAG tag on the C terminus.

Construction and Expression of Mouse ΔK-uPA Domain Deletion Mutant—The muPA/pMT/BiP plasmid encoding mouse uPA inserted between the Bgl2 (5′) and Xba1 (3′) sites used to express the recombinant WT mouse uPA in *Drosophila* S2 cell-based expression system has been described previously (41). To obtain a vector that encodes kringle-deficient muPA (ΔK-muPA), the muPA/pMT/Bip plasmid was used as a template, and an overlap PCR strategy was applied. In the first step, two fragments were generated using the primer sets 1) P1 forward (5′-CGCTCGGGAGATCTGGCAGTGTACTTGGAGC-3′) and P2 reverse (5′-CTACAGACGAAGAAGGCTTTGC-ATCTATCTCACAGTGCTkCCCCCTGGAATTTCC-3′) to generate the fragment 1.1, with the Bgl2 restriction site at the 5′ end, and 2) P3 forward (5′-GGAAATTCCAGGGGGAGCAC-TGTGAGATAGATGCAAAGCCTTCTTCGTCTGTAG-3′) and P4 reverse (5′-CGAAGGGCCCTCTAGACTATTAGAA-GGCCAGACC TTTCTCTTC-3′) to generate the fragment 1.2 having the Xba1 restriction site at the 3′ end. In the second step, the 1.1 and 1.2 fragments were mixed at an equimolar ratio, and the mixture was used as the template for the overlap PCR using the P1 forward and P4 reverse primers to generate the ΔK-muPA fragment having the Bgl2 and Xba1 restriction sites at the 5′ and 3′ ends, respectively (ΔK-muPA(Bgl2/Xba1) fragment). The muPA/pMT/BiP plasmid was cut with the Bgl2 and Xba1 restriction enzymes to remove the muPA insert, and the restricted plasmid was used to ligate the ΔK-muPA(Bgl2/Xba1) fragment to obtain the ΔK-muPA/pMT/BiP vector. This vector was then used to express the recombinant ΔK-muPA lacking amino acids 48–144 in the *Drosophila* S2 cell-based expression system as described (42).

muPA/pWPXL and ΔK-muPA/pWPXL Constructs—The QuikChange® mutagenesis kit (Stratagene) and muPA/pMT/BiP plasmid template were used to replace the BiP signal peptide in the muPA-pMT/BiP construct with the native signal peptide MKVWLASLFLCALVVKNSEG for mouse uPA in two steps. First, a pair of primers (P5 forward (5′-TTGGCCTCTC-GCTCGGGAGATCTTGCGCCTTGGTGGTGAAAAACTC-TGAAGGTGGCAGTGTACTTGGAGCTCCTGATGAA-3′) and P6 reverse (5′-TTCATCAGGAGCTCCAAGTACACTG-CCACCTTCAGAGTTTTTCACCACCAAGGCGCAAGAT-CTCCCGAGCGAGAGGCCAA-3′)) was used to replace the nucleotide sequence encoding the BiP signal sequence for the nucleotide sequence encoding CALVVKNSEG peptide at the 5′

[3] The abbreviations used are: uPA, urokinase-type plasminogen activator; uPAR, uPA receptor; scuPA, single-chain uPA; GFD, growth factor-like domain; Ab, antibody; MVEC, microvascular endothelial cell; hMVEC, human MVEC; LMVEC, lung MVEC; mLMVEC, mouse LMVEC; PRH, proline-rich homeodomain protein; EC, endothelial cell; con, control; muPA, mouse uPA; ATF, amino-terminal fragment; SM, smooth muscle.

end of the sequence encoding muPA (muPA/pMT/sign1 intermediate vector). Second, the primer pair (P7 forward (5′-GTTGGCCTCTCGCTCGGGAGATCTATGAAAGTCTGGCTGGCG AGCCTGTTCCTCTGCGCCTTGGTGGTGAAAAACTCTG-3′)) and P8 reverse (5′-CAGAGTTTTTCACCACCAAGGCGCAGAGGAACAGGCTCGCCAGCCAGACTTTCATAGATCTCCCGAGCGAGAGGCCAAC-3′)) was used to introduce the sequence encoding the MKVWLASLFL peptide into the muPA/pMT/sign2 intermediate vector, which encodes full-length mouse uPA with native signal peptide allowing the protein to be secreted in mammalian cells. The following primer pair (P9 forward (5′-GCCTAAGCTTACGCGTATGAAAGTCTGGCTGGCG-3′) and P10 reverse (5′-GTAATCCAGAGGTTGATTATCATATGACTAGTCTATTAGAAGGCCAGACCTTTCTC-3′)) was used to amplify the fragment muPA with the natural signal peptide from the muPA/pMT/sign2 intermediate vector template to introduce an MluI site in the 5′-untranslated region and an SpeI site in the 3′-untranslated region of the fragment, respectively. The fragment was cut with the Mlu1 and Spe1 restriction enzymes and then cloned into the pWPXL vector (Addgene and D. Trono laboratory, EPFL-SV-GHI-LVG, Station 19, CH-1015, Lausanne, Switzerland) and digested with MluI and SpeI to obtain the muPA/pWPXL lentiviral transfer vector, which encodes full-length mouse uPA.

To obtain the pWPXL-based lentiviral transfer vector, which encodes ΔK-muPA, the muPA/pMT/sign2 intermediate vector was used as a template, and an overlap PCR strategy was applied as described above. The P9 forward primer (5′-GCCTAAGCTTACGCGTATGAAAGTCTGGCTGGCG-3′) and the P2 reverse primer (5′-CTACAGACGAAGAAGGCTTTGCATCTATCTCACAGTGCTCCCCCTGGAATTTCC-3′) were used to generate the fragment 2.1, having the Mlu1 restriction site at the 5′ end. The P3 forward primer 5′-GGA AAT TCC AGG GGG AGC ACT GTG AGA TAG ATG CAA AGC CTT CTT CGT CTG TAG-3 and the P10 reverse primer 5′-GTAATCCAGAGGTTGATTATCATATGACTAGTCTATTAGAAGGCCAGACCTTTCTC-3′ were used to generate the fragment 2.2 having the Spe1 restriction site at the 3′ end. As above, the mixture of 2.1 and 2.2 fragments was used as the template for the overlap PCR using the P9 forward and P10 reverse primers to generate the ΔK-muPA fragment having the Mlu1 and Spe1 restriction sites at the 5′ and 3′ ends, respectively. This vector was treated with the above restriction enzymes and cloned in pWPXL vector as above to generate ΔK-muPA/pWPXL. Production of lentivirus using empty pWPXL and muPA/pWPXL or ΔK-muPA/pWPXL as transfer vectors was performed as described previously (41)

Animals

$uPA^{-/-}$ and WT mice were obtained under a Material Transfer Agreement (MTA) between the Russian Cardiology Research and Production Center (Moscow, Russia) and the FIRC Institute for Molecular Oncology (Milan, Italy). The colony was maintained at the Pushchino nursery (Pushchino, Russia). All experimental procedures were performed according to the "Rules for carrying out experiments using laboratory animals" of the Russian Cardiology Research and Production Center.

Isolation of Mouse Lung Microvascular Endothelial Cells (mLMVECs)

Mouse pulmonary microvascular endothelial cells were isolated as described (43) with minor modifications. Lung tissue obtained from 6–8-day-old WT and $uPA^{-/-}$ mouse pups was cut into pieces, digested with collagenase II/dispase (C/D) solution, and dispersed mechanically into single-cell suspensions. Lung microvascular endothelial cells (LMVECs) were purified from the cell suspension using positive selection with anti-mouse CD31 (PECAM-1) antibody MicroBeads Kit (MACS Miltenyi Biotec, catalog #130-097-418, Lot 5130819199). Cells were further purified using Dynabeads coupled to anti-mouse ICAM-2 antibody (Southern Biotech, catalog #1925-01, Lot F1912-YD13). The resultant mLMVECs exhibited a cobblestone phenotype, as visualized by phase-contrast light microscopy, and their endothelial phenotype was confirmed by fluorescence microscopy using anti-mouse CD31 antibody (BioLegend, catalog #102402, lot B128572).

Migration Assay

mLMVECs isolated from WT or $uPA^{-/-}$ mice or $uPA^{-/-}$ mLMVECs infected with control or mouse WT uPA- or mouse ΔK-uPA-encoding LVs were deprived for 24 h in EBM-2 basal medium supplemented with 0.5% FBS (EBM-2/0.5% FBS medium). Starved cells were detached by trypsin, washed, and resuspended in EBM-2/0.5% FBS. Wells in 24-well plates were filled with either EBM-2/0.5% FBS or EBM-2/0.5% FBS medium supplemented with 25 ng/ml mouse VEGF A (R&D Diagnostics). FluoroBlok™ transwell inserts (BD Biosciences) were inserted into the wells, and cell suspensions, prepared as above (5×10^4 cells/ml), were added to the transwells and allowed to migrate for 18 h per the manufacturer's instructions. No increase in total cell number was observed during this time (not shown). Migrating cells were loaded with Calcein AM dye and Hoechst33342 dye for visualization and fixed in 4% paraformaldehyde. Cells were photographed using either a Leica DM4000 inverted fluorescence microscope equipped with a 10× objective or with an EVOS® FL Auto Cell Imaging System (ThermoFisher Scientific) using a 4× objective. Cell numbers in each microscopic field were quantified using EVOS® software.

In Vitro Endothelial Cell Tube Formation Assay

mLMVECs isolated from WT or $uPA^{-/-}$ mice or $uPA^{-/-}$ mLMVECs infected with control or mouse WT uPA- or mouse ΔK-uPA-encoding LVs were studied. *In vitro* endothelial cell tube formation assay was performed and quantified as described by us previously (44–46). Movies showing time courses of endothelial tube network formation by WT and $uPA^{-/-}$ mouse ECs were taken using the EVOS® FL Auto Cell Imaging System equipped with the EVOS® Onstage Incubator.

Ex Vivo Aortic Sprouting

Thoracic aortae were isolated from 8–12-week-old mice as described by us previously (47, 48). Aortic segments were embedded into Matrigel (Corning) containing EGM with

VEGF (5 nM). Aortic ring sprouts on days 7 or 10 were fixed in 4% paraformaldehyde and photographed as below. In some experiments the samples were stained with DAPI and photographed to include all sprouts along the perimeter of the projection of the vessel ring and the entire length of the sprouts. Sprout lengths were determined by morphometric analysis using ImageJ software. To determine the entire area occupied by sprouts, several fluorescent images of the same vessel ring taken at different positions were superimposed and stitched to reconstruct the entirety of the vessel including the outgrown sprouts. Sprout areas were determined by morphometric analysis using ImageJ software and dividing the area of the sprouts by the aortic perimeter. Images of sprouting were obtained using an EVOS® FL Auto Cell Imaging System with a 4× objective or a Leica DMI6000 microscope using a 5× objective.

Proteins and Purification

Recombinant human wild type human scuPA (WT-scuPA), scuPA lacking the growth factor-like domain (GFD) (ΔGFD-scuPA, amino acids 47–411), scuPA lacking the Kringle domain (KD) (lacking amino acids 47–135; ΔK-scuPA), the N-terminal fragment of uPA, amino-terminal fragment (ATF) (GFD + KD, amino acids 1–143), and low molecular weight scuPA (amino acids 144–411) were expressed using the Drosophila Expression System (Invitrogen) in Schneider S2 cells and purified as described (42).

Immunoprecipitation and Western Blotting

HEK293 cells were transfected with HHEX-FLAG/pcDNA3.1 and uPA/pcDNA3.1 vectors as described (38). Two days after transfection, cells were harvested, and nuclear extracts were prepared using the Novagen NucBuster Protein Extraction kit. uPA and/or HHEX-FLAG were immunoprecipitated using anti-uPA mouse mAbs (IMTEK, catalog #MGH Upai) or mouse anti-FLAG mAbs (Sigma, catalog #F1804, Lot 124K6106) immobilized on agarose beads. Immunoprecipitated proteins were subjected to Western blot analysis. Immunoprecipitated and co-immunoprecipitated uPA and/or HHEX-FLAG were detected using anti-uPA rabbit polyclonal Abs (American Diagnostica, catalog #389, Lot 198) and mouse HRP-conjugated anti-FLAG M2 mAbs (Sigma, catalog #A8592, Lot 013K9167). Human LMVEC were pretreated with recombinant scuPA to allow translocation to the nucleus. Nuclear extracts were obtained as described above. uPA and endogenous HHEX were immunoprecipitated using anti-uPA mouse mAbs (as above) and anti-HHEX mouse mAbs (Santa Cruz Biotechnology, catalog #sc-81284, Lot E2015). uPA was detected as above. HHEX was detected using rabbit anti-HHEX Abs (Abcam, catalog #34222, Lot 513969).

Western blot analysis of the cell lysates was performed as described elsewhere using the following antibodies (Abs): anti-phospho$^{(Thr\text{-}202/Tyr\text{-}204)}$Erk1,2 (catalog #4370, Lot 6), anti-Erk1,2 (catalog #4695, Lot 14), anti-phospho$^{(Ser\text{-}235/236)}$S6 (catalog #4856, Lot 9), anti-S6, (catalog #2217, Lot 5) from Cell Signaling Technology, anti-VEGFR1 (catalog #32152, Lot GR140909-3) and anti-VEGFR2 (catalog #39256, Lot GR129356-1) from Abcam, and anti-GAPDH (catalog #MAB374, Lot JC1641540) from Millipore.

Transcription Factor Protein Binding Array Analysis

Binding of uPA to transcription factors was analyzed using the TranSignal™ TF Protein Array kit (Version I, catalog #MA3501, Panomics) per the manufacturer's instructions as described by us previously (38). Imaging of the membranes was performed using the ChemiDoc-It® Imaging System (UVP, LLC, Upland, CA) with the LabWorks Image Acquisition and Analysis Software (UVP Inc. Bioimaging Systems).

Indirect Immunofluorescence Staining

To analyze the intracellular distribution of exogenously added uPAs in primary human pulmonary microvascular endothelial cells (hLMVECs), the cells were grown in 8-well chamber slides (LabTek, Campbell, CA) and incubated with 20 nM WT-scuPA or ΔGFD-scuPA or ΔK-scuPA for 30 min. The cells were stained as described (37) using the anti-uPA Abs (American Diagnostica, catalog #389, Lot 198), and nuclei were counterstained with DAPI (0.5 μg/ml). Stained cells were mounted as described (37) and examined with a confocal laser-scanning microscope (Zeiss LSM 510; Carl Zeiss, Heidelberg, Germany). Images taken in DAPI channel were pseudocolored in red.

Immunohistochemistry Analysis

Paraffin-embedded sections of non-small lung carcinoma tissue were deparaffinized in xylene and rehydrated in graded ethanol solutions. Blocking of endogenous peroxidase and permeabilization was performed in 2.2% H_2O_2 solution in methanol. Permeabilized sections were blocked for 20 min using 10% horse serum diluted in 1% BSA/1× automation buffer solution (blocking buffer) at room temperature. Sections were incubated overnight at 4 °C with primary mouse monoclonal anti-human uPA Ab (American Diagnostica, catalog #3689, Lot 060406) diluted in the blocking buffer, washed, and incubated with biotinylated horse anti-mouse secondary Ab diluted in the blocking buffer for 30 min at 37 °C followed by incubation with streptavidin-HRP (Vectastain kit; Vector). The tyramide signal amplification (TSA) reaction was performed using Alexa 488 Fluor TSA kit (Invitrogen) as per the manufacturer's instructions. Tissue sections were then incubated with Cy3-conjugated mouse monoclonal anti-SM α-actin Ab (Sigma, catalog #C6198, Lot 024M4838V) in blocking buffer for 1 h. The slides were incubated with SYTO-6 fluorescent dye (Invitrogen) to visualize the nuclei, mounted in Gel-Mount medium (Electron Microscopy Sciences, Hatfield, PA), and analyzed using confocal microscopy, as above. Images taken in far-red channel for nuclear staining (SYTO-6 stain) were pseudo-colored in red. Images taken in red channel (Cy3-conjugated anti-SM α-actin) were pseudocolored in blue.

Immunohistochemical staining of sections was performed for the endothelial cell marker von Willebrand factor. Fresh specimen sections and de-mounted sections previously stained for uPA and SM α-actin were subjected to antigen retrieval using Dako Target Retrieval Solution after blocking of endogenous peroxidase as above. Sections were blocked using 10% goat serum diluted in 1% BSA/1× automation buffer and incu-

bated overnight at 4 °C with primary rabbit polyclonal anti-von Willebrand factor Ab (Dako, catalog #A008229–5, Lot 20020455) or whole rabbit Ig as a negative control. Subsequent staining steps were as above except that 3,3′-diaminobenzidine (Thermo Fisher) was used as an HRP substrate, and nuclei were counterstained with hematoxylin solution (Thermo Fisher). Images were taken using EVOS® FL Auto Imaging System.

Solid Phase Protein-Protein Binding Assay

To study HHEX-FLAG binding to uPA deletion mutants, 96-well plates were coated with 0.7 μM each of recombinant uPA deletion mutant or 1% BSA in Dulbecco's modified PBS, blocked with Dulbecco's modified PBS supplemented with 1% BSA, and incubated with the nuclear extract from 293HEK cells transfected with the HHEX-FLAG-pcDNA3.1 construct for 1 h. After washing with Dulbecco's modified PBS supplemented with 1% BSA, bound HHEX-FLAG was detected using anti-HHEX rabbit polyclonal Ab (Abcam, catalog #34222 Lot 513969) followed by incubation with HRP-conjugated anti-rabbit antibody (Jackson ImmunoResearch Laboratories, catalog #111-035-144) and color development with 3,3,5,5-tetramethylbenzidine. The reaction was terminated by adding 1 mM H_2SO_4, and the absorbance at 450 nm was measured using a microplate reader.

Cell Proliferation Assay

Proliferation of human LMVECs (Lonza) was measured using the [^{3}H]thymidine incorporation assay as described (49). Briefly, cells were plated at 60% confluency in EGM-2 complete medium (Invitrogen), starved in EBM-2 medium containing 0.5% FBS and antibiotic/antimycotic supplement (EBM-2/0.5% FBS) (Invitrogen) for 24 h, and stimulated with human VEGF (R&D Diagnostics) in EBM-2, 0.5% FBS for an additional 24 h. [^{3}H]Thymidine was added during the last 3 h of incubation of the cells with VEGF (final concentration 1 μCi/ml), the cells were washed to remove unincorporated [^{3}H]thymidine and harvested, and the incorporated radioactivity was quantified as described (49). Proliferation of mouse LMVECs was measured using the BrdU incorporation assay as described (50) with several modifications; cells were plated in black 96-well plates with clear bottoms, and Alexa488-conjugated secondary Ab was used to detect bound anti-BrdU antibodies. Fluorescence was measured using the Synergy™ 2 Multi-Detection Microplate Reader (BioTek Instruments, Inc.) and analyzed using the Gen5™ Microplate Data Collection & Analysis Software.

Electrophoretic Mobility Shift Assay (EMSA)

HEK293 cells were transfected with HHEX-FLAG in pcDNA3.1 vector. Two days after transfection, cells were harvested, and nuclear extracts were prepared using the NucBuster Protein Extraction kit (Novagen, Gibbstown, NJ). EMSA reactions were performed using biotinylated double-stranded oligonucleotide derived from VEGFR2 promoter, 5′-ACCAGATTCAGCTTTTTAAACTACAATTATACTG-3′, and the LightShift chemiluminescence EMSA kit (Pierce, Rockford, IL), as described (38). uPA or BSA (500 ng/reaction) was added to the binding reaction where indicated.

VEGF R1 and R2 Promoters Reporter Assay

Promoter reporter assay was performed using co-transfection of 1.3 kb VEGFR2 promoter luciferase reporter in pGL3 vector (Promega) (VEGFR2-pGL3) and 1.2-kb VEGFR1-pGL3 (51), uPA/pcDNA3.1, and HHEX-FLAG/pcDNA3.1 in EA.hy926 cells as described by us previously (51) with the exception that HHEX-FLAG/pcDNA3.1 vector was used instead of pMUG1-Myc-PRH, and pRL-CMV vector (Promega) was co-transfected together with VEGFR1-pGL3 or VEGFR2-pGL3 to normalize transfection efficiency using a Dual Luciferase reporter assay kit (Promega).

Quantitative Reverse Transcriptase-mediated PCR

K562 cells (1×10^7) were transfected with 10 μg of pMUG1-PRH or pSIH-uPA and empty pMUG1 and pSIH plasmids for 48 h. RNA was produced according to standard protocols. Quantitative PCR was performed in triplicate as described (51) using the primers listed below, and the data were analyzed using Rotorgene 6 software (Corbett Research; Rotorgene RG-3000). Glyceraldehyde-3-phosphate dehydrogenase (GAPDH) was used as the internal control. Results for relative expression ratios were calculated according to the efficiency calibrated mathematical model.

The primers used were as follows: *Vegfr-1* forward, 5′-TGGCCATCACTAAGGAGCACTCC-3′, and reverse, 5′-GGAACTGCTGATGGCCACTGTG-3′; *Vegfr-2* forward, 5′-TTAGTGACCAACATGGAGTCGTG-3′, and reverse, 5′-TAGTAAAGCCCTTCTTGCTGTCC-3′; and GAPDH forward, 5′-TGATGACATCAAGAAGGTGGTGAAG-3′, and reverse, 5′-TCCTTGGAGGCCATGTGGGCCAT-3′.

Statistical Analysis

Differences between groups were compared using the one-way analysis of variance statistical test. Statistical analyses were performed using the EZAnalyse add-in to Microsoft Excel software. Significance was set at a p value of <0.05.

Results

uPA Is Required to Induce Angiogenesis by VEGF in Vivo—To further assess whether uPA is involved in VEGF-induced angiogenesis (33, 52), we first asked if uPA modulates VEGF-induced capillary sprouting using aortic rings isolated from WT and uPA$^{-/-}$ mice. Aortae from WT mice embedded in Matrigel developed sprouts in response to VEGF that were >3 times longer those emanating from the aortae of uPA$^{-/-}$ mice (7.01 ± 0.24 *versus* 2.32 ± 0.15, respectively) ($p < 0.001$) (Fig. 1*A*). The lengths of the sprouts developed from unstimulated WT aortae were 1.43 times longer those from uPA$^{-/-}$ mice ($p < 0.001$) (Fig. 1*B*), suggesting additional growth factors in Matrigel that affect sprouting also depend on uPA, although not to the same extent as VEGF.

uPA Potentiates VEGF-induced Microvascular Endothelial Cell Proliferation, VEGF-induced Signaling, and Migration—Angiogenesis requires that endothelial cells proliferate and migrate. To examine the role of uPA in VEGF-induced EC proliferation, mLMVECs from uPA$^{-/-}$ and WT mice (53) were incubated with VEGF. VEGF (10 ng/ml) induced a >3-fold

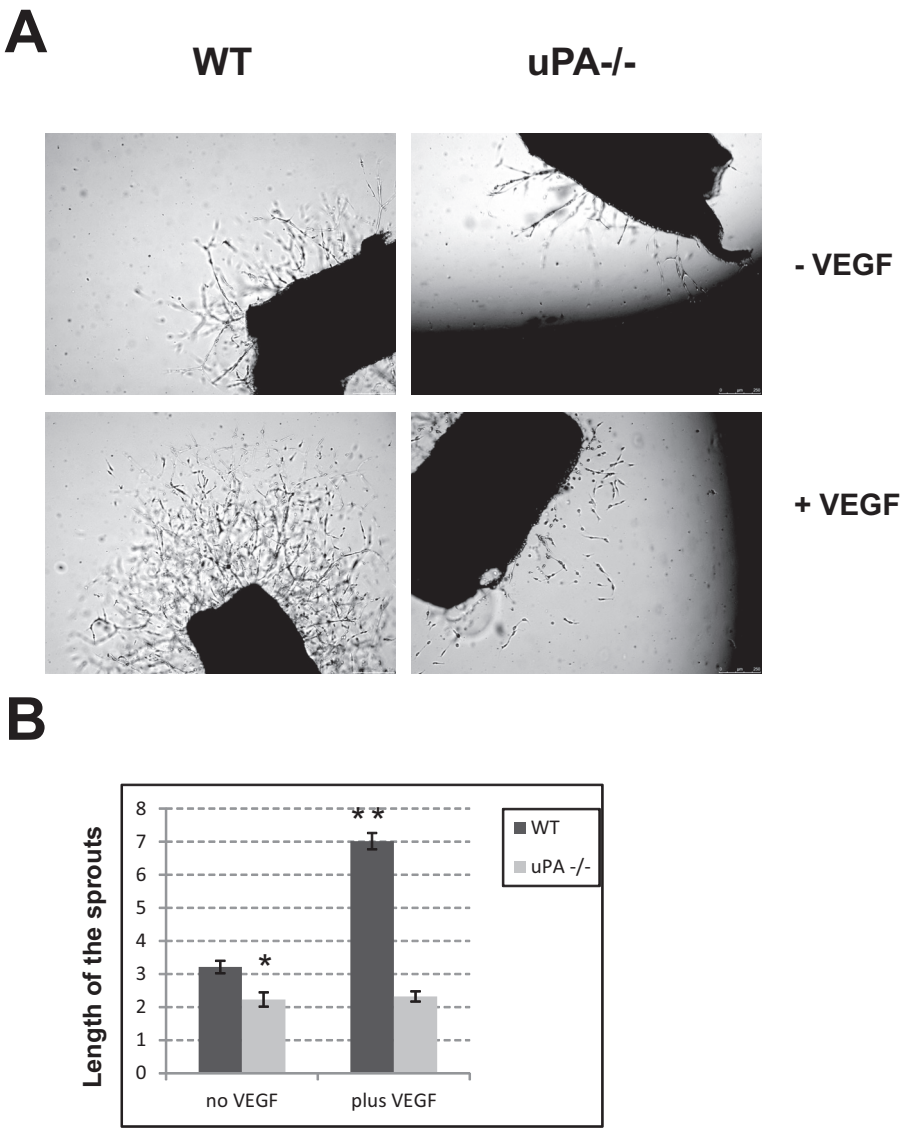

FIGURE 1. **Vascular response to VEGF in WT and uPA KO (uPA$^{-/-}$) mice.** *A*, sprouting from the aortae of WT or uPA$^{-/-}$ mice. Sprouting was stimulated with VEGF (5 ng/ml) in EGM-2 medium (VEGF-depleted EGM-2 medium served as a negative control). Representative images from 6 experiments under each of the conditions are shown taken at day 7 post embedding of the vessel rings into Matrigel. *B*, *bar graph* showing the length of sprouts (mean ± S.E.) from the aortae of WT or uPA$^{-/-}$ mice after stimulation with VEGF (100 ng/ml). Results are representative of two independent experiments. *, $p < 0.05$ for untreated WT versus uPA$^{-/-}$ samples. **, $p < 0.001$ for untreated WT versus VEGF-treated WT samples.

increase in DNA synthesis in WT mLMVEC, whereas uPA$^{-/-}$ mLMECs were almost completely non-responsive (Fig. 2*A*). uPA$^{-/-}$ mLMVECs were then transfected with a lentiviral construct encoding mouse uPA (KO EC uPA LV) or with empty lentiviral construct as a negative control (KO EC con LV). Transfected cells were then stimulated with 5–25 nM mouse VEGF for 18 h. KO EC uPA LV showed significantly greater proliferation in response to VEGF than did KO EC con LV cells ($p < 0.001$) (Fig. 2*B*). Erk1,2 and PI3K-Akt-S6K pathways are activated in endothelial cells stimulated by VEGF (54–56) and have been implicated in mediating proliferative responses in endothelium (57, 58) and in other cell types (for review, see Ref. 59). VEGF induced sustained phosphorylation of Erk1,2 and the S6 ribosomal subunit (the substrate of p70 S6 kinase, one of the effectors of the PI3K/Akt/mTOR pathway; Ref. 60) in KO EC uPA LV within 2 min, whereas either delayed phosphorylation of Erk1,2 (after 10 min of stimulation) or almost no S6 ribosomal subunit phosphorylation was seen in the KO EC con LV cells (Fig. 2*C*). uPA also potentiated the proliferative response of human LMVECs to VEGF (Fig. 2*D*).

We also compared migration of mLMVEC isolated from WT and uPA$^{-/-}$ mice in response to VEGF. Unstimulated WT and uPA$^{-/-}$ cells showed little or no migration through the porous membrane (Fig. 3*A*). When stimulated with VEGF (25 ng/ml), the migration response of WT mLMVEC was >3 times greater than uPA$^{-/-}$ LMVEC.

We then utilized an *in vitro* endothelial tube formation assay to compare angiogenic activity of WT and uPA$^{-/-}$ mLMVECs. Although WT mLMVEC formed branching endothelial tubes, uPA$^{-/-}$ mLMVEC formed clusters with few branches (Fig. 3*B*). Time-lapse videomicroscopy revealed that random migration of uPA$^{-/-}$ mLMVEC was slower than WT cells, and although there was some evidence of elongation, the intercellular con-

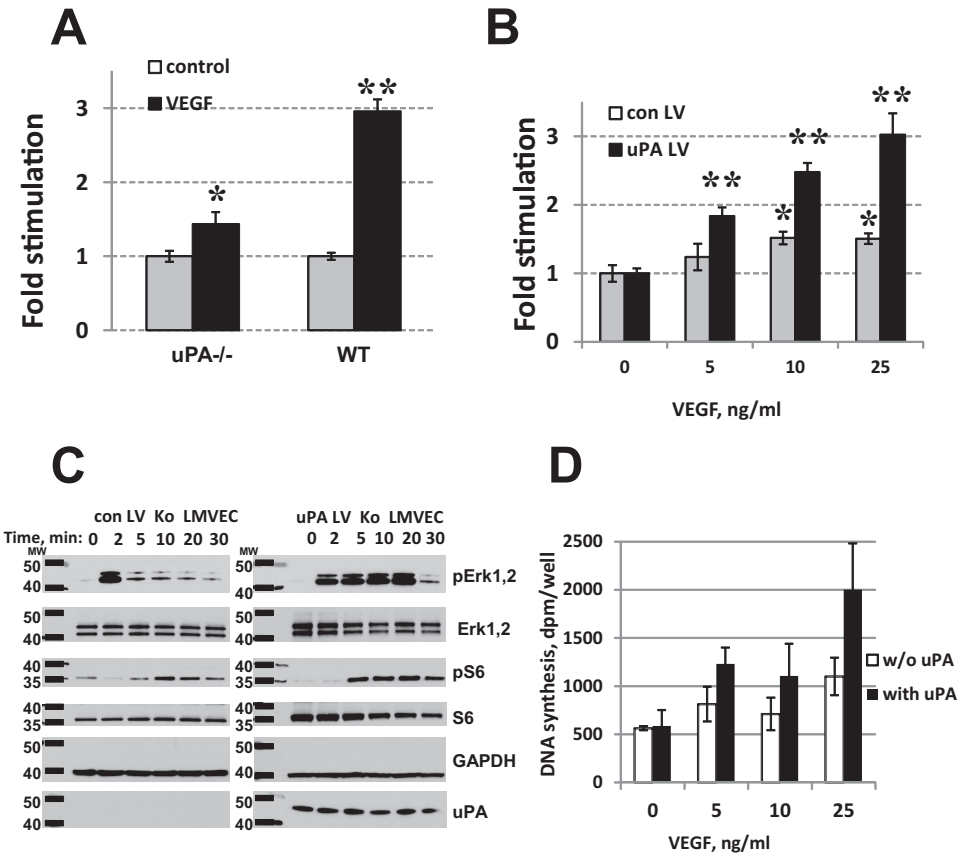

FIGURE 2. **Stimulation of mitogenesis in endothelial cells by VEGF-A requires uPA.** *A*, DNA synthesis in response to VEGF in LMVECs isolated from WT or uPA$^{-/-}$ mice. Endothelial cells were plated in 96-well plates, cultured for 24 h in complete medium, starved in 1% FBS/EBM for 24 h, and then stimulated with VEGF (25 ng/ml) for an additional 24 h. DNA synthesis was assessed by measuring incorporation or 5-ethynyl-2′-deoxyuridine. *y* axes denote -fold stimulation of DNA synthesis in response to VEGF relative to untreated cells (1-fold). The results, representative of one of three independent experiments performed in triplicate, are shown as the mean ± S.E. *B*, re-expression of uPA in uPA$^{-/-}$ endothelial cells restored DNA synthesis in response to VEGF. uPA$^{-/-}$ LMVEC transfected either with "empty" (*con*) LV or uPA-bearing LVs were plated in 96-well plates, cultured, and serum-deprived as in *Panel A*. VEGF was added for 24 h at the indicated concentrations, and DNA synthesis was measured as in *panel A*. *x* axes denote concentrations of VEGF in ng/ml. *y* axes denote -fold stimulation of DNA synthesis in response to VEGF relative to untreated cells (1-fold). Data from three independent experiments performed in triplicate are shown as the mean ± S.E. * denotes $p < 0.05$, ** denotes $p < 0.001$. *C*, re-expression of uPA in uPA$^{-/-}$ endothelial cells amplified VEGF-induced signaling. uPA$^{-/-}$ LMVEC were transfected with empty (*con*) LV or uPA-bearing LV, starved overnight, and lysed at the indicated times after stimulation with VEGF (10 ng/ml). Western blot analysis shows the time course of ERK1/2 and ribosomal S6 unit phosphorylation, which reflects activation of the PI3k/Akt/mTOR/S6 Kinase (S6K) pathway (60). Anti-GAPDH was used to ensure equal protein loading. The illustrated blots are representative of three independent experiments. *D*, uPA potentiates DNA synthesis in response to VEGF in hLMVECs. hLMVEC were plated in 48-well plates, cultured for 24 h in complete medium, starved in 1% FBS/EBM for 24 h in the absence or presence of 20 nM uPA, and stimulated with VEGF at the indicated concentrations for an additional 24 h. DNA synthesis was assessed by measuring [^{3}H]thymidine incorporation into DNA. Data are representative of three experiments performed in triplicate are shown as mean ± S.E.

nections were unstable (supplemental Movie 1). In contrast, cells isolated from the WT mice readily formed tubular network structures (supplement Movie 2).

uPA Translocates to the Nucleus of Endothelial Cells—uPA is secreted as a scuPA (61, 62) that is able to bind uPAR (12) and other receptors (14, 63) and can be converted into a two-chain active enzyme by plasmin and some other proteases (64). We previously reported that scuPA, but not two-chain uPA (*tcuPA*) or a kringle-deficient uPA mutant (ΔK-scuPA) (See Fig. 4*A* for schematic representation of uPA variants), translocates rapidly to the nuclei of diverse types of proliferating cells in a kringle-dependent, uPAR-independent, manner (37). To determine which scuPA variants translocated to the nuclei of human LMVECs, WT-scuPA, ΔGFD-scuPA, and ΔK-scuPA were radiolabeled with Na^{125}I and incubated with hLMVECs for 1 h. Exogenously added recombinant ^{125}I-scuPA and ^{125}I-ΔGFD-scuPA, but not ^{125}I-ΔK-scuPA, translocated to the nuclei of proliferating hLMVECs (Fig. 4*B*). Fig. 4*C* shows the subcellular distribution and immunofluorescence labeling of exogenously added unlabeled scuPA, ΔGFD-scuPA variant, that does not bind uPAR (37, 42) but retains the kringle and translocates to the nuclei of endothelial cells and ΔK-scuPA variant. Untreated hLMVECs are shown in the *right panel*. These data confirm that uPAR is not essential for nuclear translocation of the kringle-containing WT uPA or its variant in lung microvascular endothelial cells.

To assess the relevance of this observation, we next asked whether endogenous uPA is present within the nuclei of endothelial cells *in situ*. Using confocal microscopy, we found that uPA is present within the nuclei of endothelial cells (marked by *closed arrowheads*) lining angiogenic vessels as well as within the nuclei of tumor cells (not shown) in a specimen of non-small lung carcinoma (Fig. 5, *A* and *B*). Not all nuclei stain for uPA, even in cells that express cytoplasmic or cell surface uPA. This suggests that the appearance of uPA within the nucleus might be under spatial or cell cycle control.

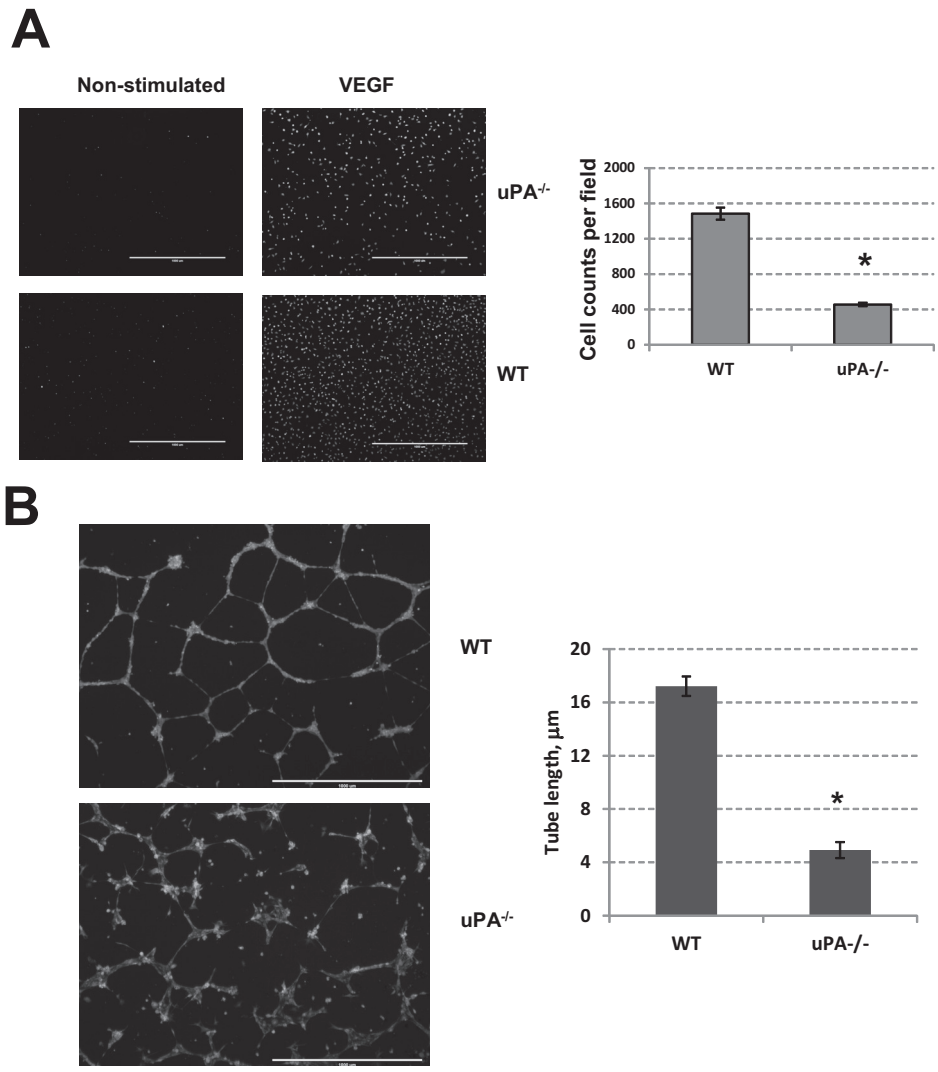

FIGURE 3. **EC migration and *in vitro* tube formation in response to VEGF requires uPA.** *A*, migration of lung microvascular ECs isolated from WT or uPA$^{-/-}$ mice in response to VEGF. LMVECs were starved in EBM-2/0.5% FBS for 24 h, detached with trypsin/EDTA, washed in starvation medium, and resuspended in the same medium. Cell suspensions were added inside Fluoroblok™ transwells, which were placed in 24-well plates containing either starvation medium or the same medium supplemented with 25 ng/ml VEGF. Transwells were incubated with calcein AM and Hoechst to visualize migrating cells and then fixed. Cells were allowed to migrate for 18 h and were then photographed with a 4× objective using the EVOS FL Auto Imaging System microscope. Cells within the imaged field were counted. Each condition was set up in three wells, and three images were taken at different sites within each transwell. Typical images for each condition are shown. The *bar graph on the right* shows the mean ± S.E. cell numbers per microscopic field of WT or uPA$^{-/-}$ cells that migrated in response to VEGF. Few cells migrated in starvation medium (two-three per microscopic field) and, therefore, do not appear on the graph. *, $p < 0.001$. *B*, tubular network formation by WT and uPA$^{-/-}$ ECs in response to VEGF. WT and uPA$^{-/-}$ ECs were allowed to adhere and migrate within a 24-well plate coated with Matrigel. The endothelial cell network was visualized by loading the cells with Calcein AM dye (4 μg/ml), and photographs were taken using an EVOS® FL Auto Imaging System microscope. Typical images for each condition are shown on the *left*. Total length of the tubes was enumerated using the ImageJ software. *, $p < 0.001$ (*right*).

uPAs That Are Capable of Translocation to Nuclei Up-regulate Expression of VEGFR1 and VEGFR2—Binding of VEGF-A to VEGFR1 (Flt1) and VEGFR2 (KDR) has been implicated in pro-mitogenic signaling in endothelial cells (for review, see Ref. 65). Having observed that VEGF induces a greater proliferative response in uPA-expressing ECs, we next asked whether these cells express higher levels of VEGFR1 and VEGFR2 and whether intranuclear uPA is responsible for this phenotype. To do so, we first compared the expression levels of VEGF receptors in mouse LMVECs isolated from WT and uPA$^{-/-}$ mice and in uPA$^{-/-}$ LMVECs transfected with LV vectors encoding mouse WT or ΔK-uPA (KO EC uPA LV and KO EC ΔK-uPA LV, respectively) or empty vector as the negative control (KO EC con LV). WT LMVEC and KO EC uPA LV cells showed higher expression levels of VEGFR1 and VEGFR2 than their uPA$^{-/-}$ counterparts or KO EC ΔK-uPA LV cells (Fig. 6*A*), which expressed a variant that is unable to translocate to the nucleus (Fig. 4*B* and Ref. 37). The addition of recombinant WT-scuPA and ΔGFD-scuPA, but not ΔK-scuPA (10 nM), to hLMVECs for 24 h up-regulated VEGFR1 and VEGFR2 expression (Fig. 6*B*). Together, these data suggest that only uPA variants capable of translocation to nuclei up-regulate expression of VEGFR1 and VEGFR2.

Nuclear uPA in EC Enhances VEGF-induced Angiogenic Responsiveness—To relate increased expression of VEGF receptors in response to intranuclear uPA to the angiogenic potential of ECs, we re-expressed either WT-uPA or ΔK-uPA variants in uPA$^{-/-}$ mLMVECs and studied their migration and

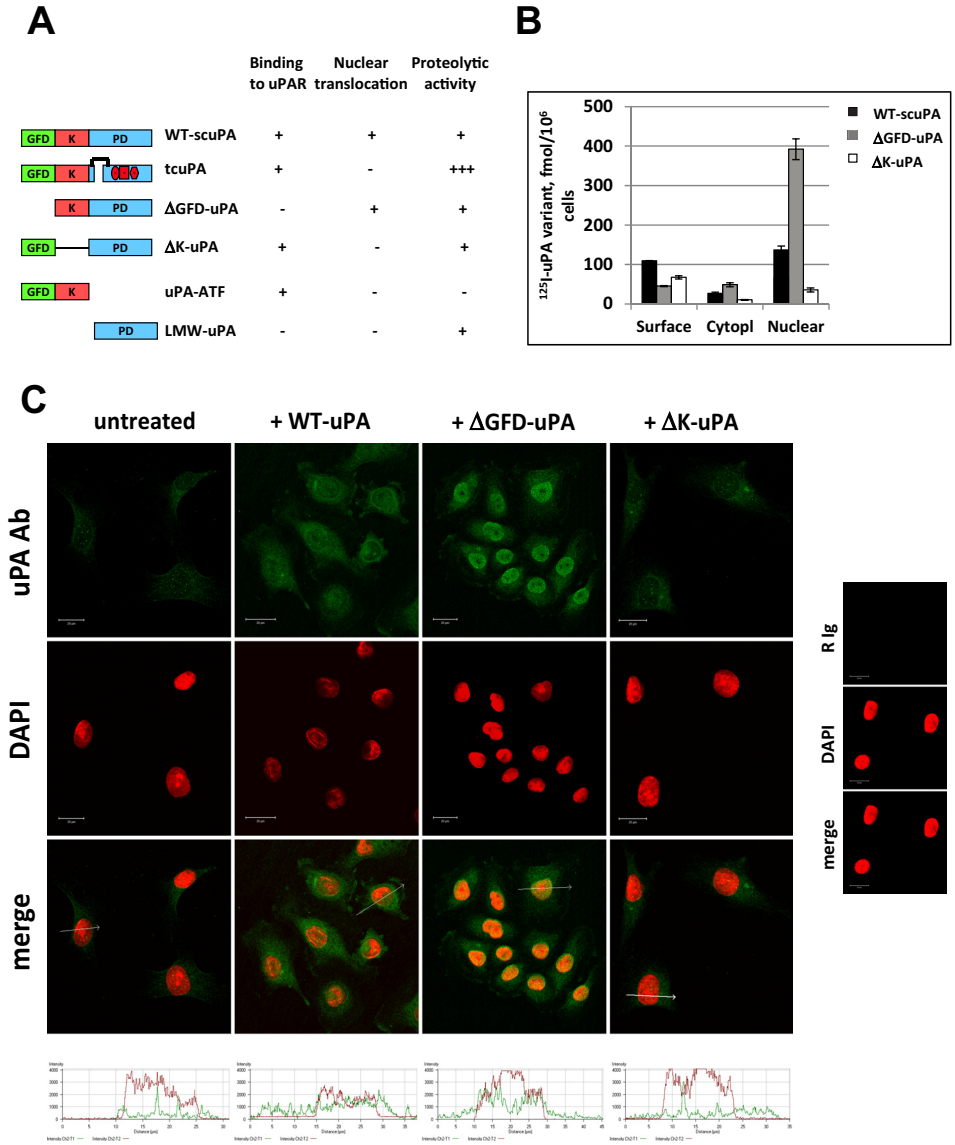

FIGURE 4. *A*, Schematic representation of uPA variants and their relevant properties. *WT*, wild type; *tcuPA*, two-chain uPA; *K*, kringle; *PD*, protease domain, Δ*GFD-uPA*, GFD-deficient uPA; Δ*K-uPA*, Kringle-deficient uPA; *LMW-uPA*, low molecular weight (*LMW*) uPA missing the GFD and Kringle domains; ATF-uPA, N-terminal fragment of uPA consisting of the GFD and the kringle. *B*, nuclear translocation of uPA in hMLVEC depends on its kringle domain. Recombinant WT-uPA and ΔK-uPA, isotopically labeled with $Na^{125}I$ as described (37), were incubated with hMVLEC for 1 h. Cells were then washed to remove unbound radioactive proteins and fractionated, and membrane-, cytoplasm- and nucleus-associated uPAs were quantified (37). Results are presented as the amount (fmol) of each protein found in each cellular fraction (membrane-bound, cytoplasmic, and nuclear) obtained from 10^6 cells. All experiments were performed in triplicate. *, $p < 0.05$. *C*, nuclear localization of exogenously added WT-uPA, ΔGFD-uPA, and ΔK-uPA in hLMVEC (*left panel*). Cells growing exponentially on 8-well chamber slides were incubated with recombinant WT-uPA or ΔGFD-uPA or ΔK-uPA (10 nM) for 1 h, washed, and fixed in MeOH. uPA was detected using immunofluorescence as described under "Experimental Procedures" and in Stepanova *et al.* (37) with anti-uPA rabbit polyclonal antibodies and Alexa 488-conjugated secondary anti-rabbit antibodies. Nuclei were counterstained with DAPI and pseudo-colored in *red*. *Green* denotes positive staining for uPA. Nuclear localization of anti-uPA antibody-positive staining was quantified using Zeiss LSM 5 Image software. The *white arrow* (*merge panels*) was used to denote the profile quantified by the LSM 5 Image software. A graphic representation of the quantitative analysis of this profile for each treatment is shown on the *bottom of the collage*. The *right panel* shows staining obtained when control rabbit Ig (*R Ig*) was used as a negative control. *Scale bar*, 20 μm.

in vitro tube formation in response to VEGF. Fig. 6*C* shows that re-expression of WT-uPA caused a 2.48-fold increase in migration of $uPA^{-/-}$ mLMVECs ($p < 0.01$), whereas expression of ΔK-uPA caused only a 1.37-fold (although significant, $p < 0.01$) increase in migration compared with $uPA^{-/-}$ mLMVEC transfected with empty lentivirus. ΔK-uPA-transfected $uPA^{-/-}$ mLMVECs, like cells transfected with empty vector, formed cell clusters in the presence of VEGF in lieu of a tubular network (Fig. 6, *D* and *E*), whereas WT-uPA-expressing cells formed tubular network structures similar to WT mouse mLMVECs (Fig. 6, *D* and *E*, with reference to Fig. 3*B*).

We then asked if the capacity of WT-uPA to translocate to the nucleus is involved in aortic sprouting. Aortic rings isolated from $uPA^{-/-}$ mice were transfected with WT-uPA, ΔK-uPA, and empty control pWPXL-based LVs immediately after isolation and embedded in Matrigel 24 h later. The parental pWPXL vector-based LV, which encodes GFP, was used to elucidate transfection efficiency of vessel ring tissues by LV. Fig. 7*A* shows that GFP was effectively delivered by LV. RT PCR analysis of the vessel rings transduced with the empty and WT-uPA- or ΔK-uPA-encoding LVs confirmed transfection (Fig. 7*B*). VEGF induced intense sprouting from the

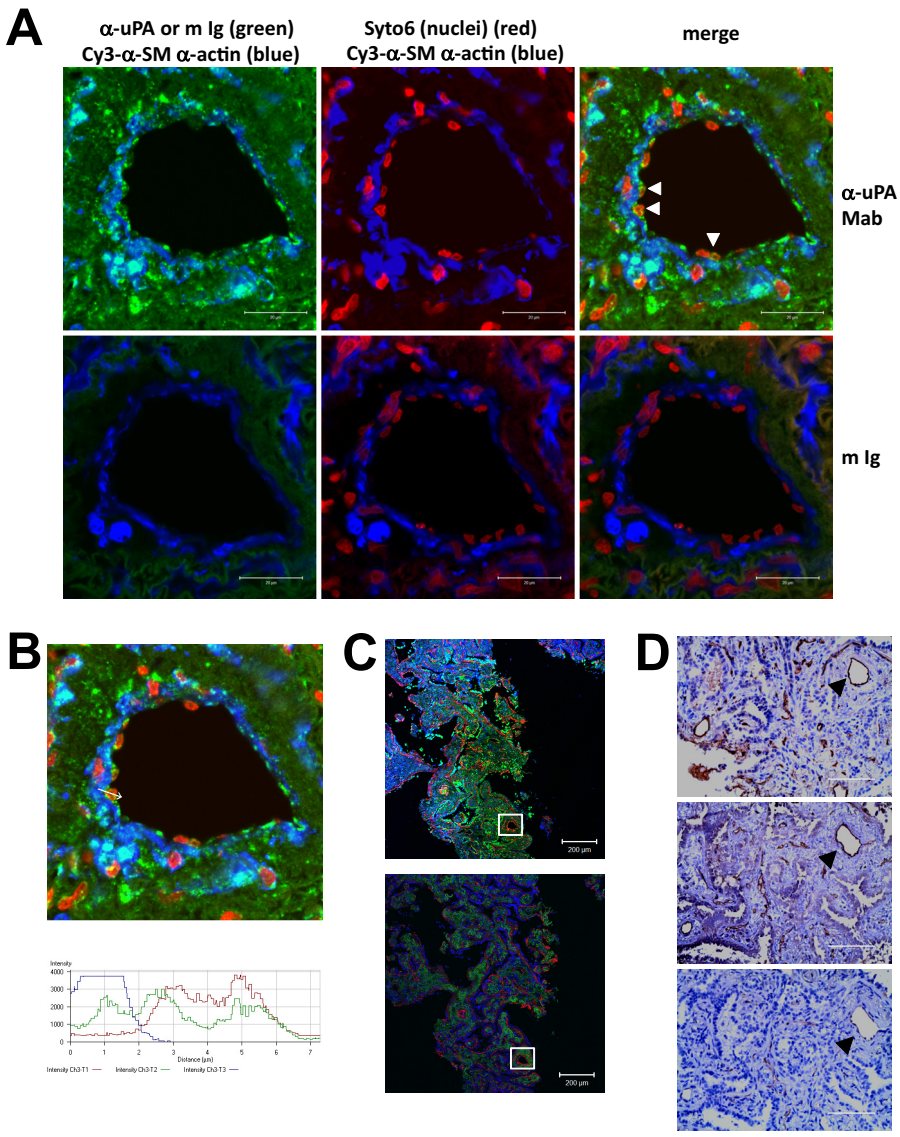

FIGURE 5. **Nuclear localization of uPA *in situ*.** *A*, staining of tissue specimens for uPA and SM α-actin. Paraffin-embedded sections of non-small human lung carcinoma tissue were stained with anti-uPA monoclonal antibody (*top panels*) or with mouse IgG_1 (*m Ig*) as a negative control (*bottom panels*), depicted in *green*. Nuclei were counterstained with SYTO-6 (pseudo-colored in *red*). Smooth muscle *a*-actin was stained using Cy3-conjugated mouse monoclonal antibody to localize vessels and airways in tissue specimen (pseudocolored in *blue*). Examples of nuclear localization of uPA in vascular ECs are denoted by *white arrowheads*. Immunostaining was analyzed using a confocal microscope ZEISS LSM 510 using a 40× objective. *Scale bar*, 20 μm. *B*, quantitation of nuclear localization of uPA. Nuclear localization of anti-uPA antibody was quantified using Zeiss LSM 5 Imaging software. The *white arrow* (*top image*) is used to denote the profile quantified by the LSM 5 Image software. A graphic representation of the quantitative analysis of this profile is shown on the bottom. *C*, low magnification Images of *A*. Images are of the same area taken using the 10× objective. The *upper panel* shows staining for uPA, smooth muscle actin, and nuclei. The *lower panel* shows staining using control rabbit Ig instead of anti-uPA antibodies (negative control). *Scale bar*, 200 μm. *Squares* indicate areas taken for magnification. *Panel D*, immunohistochemical staining of the tissue sections for the endothelial cell marker von Willebrand factor. The slide stained for uPA was dismounted and used together with intact parallel sections for immunostaining using rabbit polyclonal anti-von Willebrand factor antibody to assess whether uPA was detected in the nuclei of endothelial cells of the vessels within tumor tissue as described under "Experimental Procedures." Total rabbit Ig served as a negative control. The *brown* color (*top* and *middle panels*) denotes vascular endothelial cells; nuclei are depicted in *blue*. Images of the same vessel as in *A*, marked by *black arrowhead* in the section previously stained for uPA and in the fresh serial section, are shown in the *top* and *middle panels*, respectively. The *bottom panel* represents a negative control using a fresh serial section. Images were taken using the EVOS® FL Auto Imaging system using a 40× objective. *Scale bar* = 100 μm.

aortae expressing WT-uPA, whereas significantly less sprouting was observed from the rings expressing ΔK-uPA or transfected with empty LV (Fig. 7, *C* and *D*). These data indicate that ΔK-uPA, which does not translocate to the nucleus, are unable to fully restore angiogenic capacity to $uPA^{-/-}$ ECs in response to VEGF in contrast to WT-uPA, which invests $uPA^{-/-}$ ECs with a responsiveness comparable to ECs isolated from WT mice (Fig. 1).

Intranuclear uPA Binds to HHEX/PRH Transcription Factor and Abolishes Repression of vegfr1 and vegfr2 Promoters—We recently reported that uPA binds several homeobox transcription factors, including HOXA5 and Hey (38), that might be involved in regulating VEGFR1 and VEGFR2 expression (39, 40). Using a transcription factor protein-protein microarray, we found that uPA also binds to HHEX/PRH transcription factor (Fig. 8*A*). We previously reported that HHEX/PRH binds to

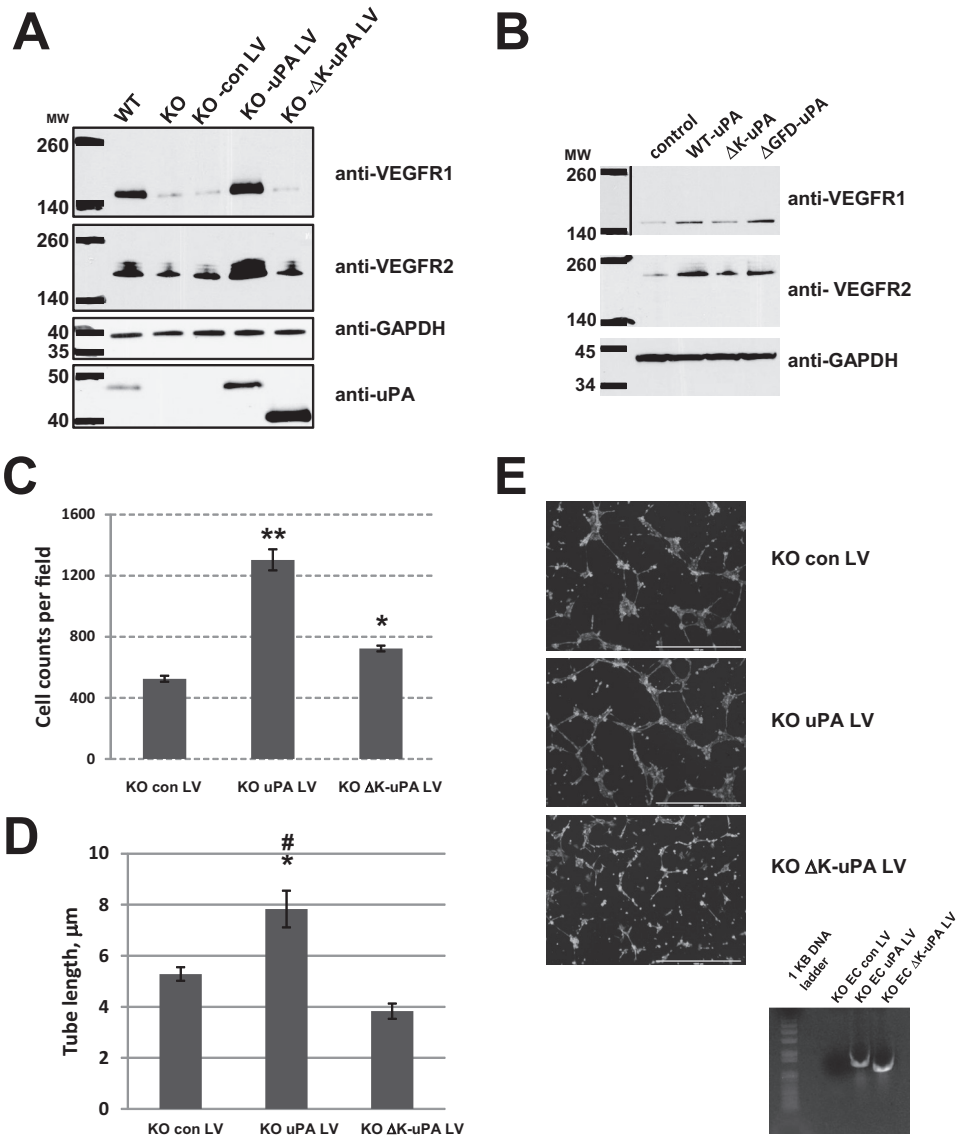

FIGURE 6. **Overexpression of VEGFR1 and VEGFR2 induced by nuclear uPA mediates increased angiogenic capacity of endothelial cells in response to VEGF.** *A*, WT mouse LMVEC and uPA-LV-KO-LMVEC but not ΔK-uPA-LV-KO-LMVEC express higher levels of VEGFR1 and VEGFR2. Lung microvascular endothelial cells isolated from WT or uPA$^{-/-}$ mice (uPA$^{-/-}$ LMVEC) or uPA$^{-/-}$ LMVEC transfected either with empty LV, full-length mouse uPA-encoding LV, or ΔK-uPA-encoding LV were lysed. The lysates were subjected to SDS-PAGE and Western blot analysis. Membranes were probed with anti-VEGFR1 and VEGFR2 antibodies. Membranes probed with the anti-GAPDH antibodies served as the loading control. The illustrated blots are representative of three independent experiments. *B*, uPA variants capable of nuclear translocation induce VEGFR1 and VEGFR2 expression in human lung microvascular endothelial cells. hMVECs were plated in EBM-2 medium supplemented with 5% FBS and growth supplements, starved in EBM-2/1% FBS for 24 h, and stimulated with 20 nM recombinant full-length human uPA (WT-uPA), GFD-deficient uPA variant (ΔGFD-uPA), or Kringle-deficient uPA (ΔK-uPA). VEGFR1, VEGFR2, and GAPDH expression was analyzed as above. The blots shown are representative of three independent experiments. *C*, re-expression of WT-uPA but not ΔK-uPA in EC isolated from uPA$^{-/-}$ mice significantly increases migration in response VEGF. ECs isolated from uPA$^{-/-}$ mice were transfected with LVs encoding either mouse WT-uPA or the ΔK-uPA variant. Cell migration was assayed as described in Fig. 3*A*. The *bar graph* shows cell numbers (mean ± S.E.) per microscopic field for uPA$^{-/-}$ ECs transfected with empty, WT-uPA, or ΔK-uPA-encoding LV migrated in response to VEGF. Few cells migrated in starvation medium (2–3 cells per microscopic field), and therefore, the numbers do not appear on the graph. *, $p < 0.01$ for values for KO con LV cells *versus* values for KO DK-uPA LV cells , **, $p < 0.01$ for values for KO WT uPA cells *versus* values for KO con LV. *D*, formation of tubular network in response to VEGF by uPA$^{-/-}$ ECs in which WT-uPA or ΔK-uPA variants were re-expressed. ECs were set up for *in vitro* tube formation as in Fig. 3*B*. Cells were incubated for 22 h and photographed at the end of incubation using the EVOS FL Auto Imaging System. Three wells were set up per each cell type, and three locations within each well were photographed. Typical pictures for uPA$^{-/-}$ EC transfected with empty LV (KO EC con LV), LV encoding mouse WT-uPA (KO EC uPA LV), and mouse ΔK-uPA (KO EC ΔK-uPA LV) are presented. Images were analyzed using ImageJ software. The *bar graph* shows quantitative analysis of the total tube lengths within the tubular network (mean ± S.E.). *, $p < 0.01$, values for KO con LV cells *versus* KO uPA LV Cells, #, $p < 0.001$, for values for KO uPA LV cells *versus* KO DK-uPA LV cells. *E*, typical images for each condition quantified in *D*. *Inset*, RT PCR analysis of the total RNA samples isolated from the empty and WT-uPA- and ΔK-uPA-LV-transfected uPA$^{-/-}$ LMVECs.

the promoter regions of the VEGFR1 and VEGFR-2 genes and represses their transcription (51). Therefore, we next tested the hypothesis that intranuclear uPA de-represses *vegfr1* and *vegfr2* promoters by binding to HHEX. In support of this hypothesis, uPA co-immunoprecipitated with HHEX/PRH when both proteins were overexpressed in 293HEK cells (Fig. 8*B*). As quiescent ECs typically express low levels of uPA, to determine if uPA co-immunoprecipitates with endogenous HHEX, we pre-incubated hMVEC with recombinant scuPA. HHEX co-immunoprecipitated with uPA from scuPA-treated hMVECs (Fig. 8*C*). We then used a series of uPA domain deletion mutants listed in Fig. 4*A* to determine which domain(s) is required for

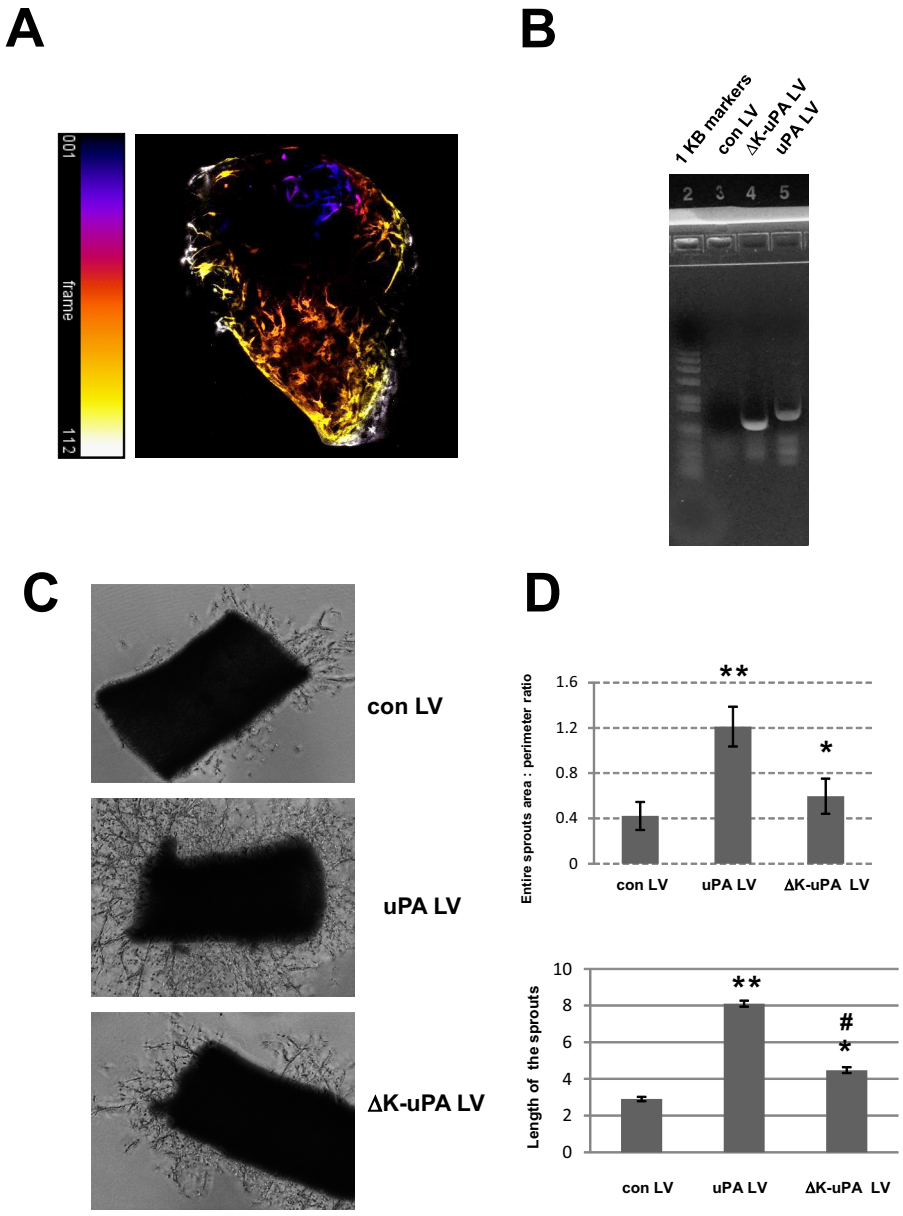

FIGURE 7. **Sprouting in response to VEGF from the aortae of uPA$^{-/-}$ mice transfected with empty, WT-uPA, and ΔK-uPA LVs.** *A*, aortic ring transfected with control pWPXL vector-based LV, which encodes GFP. Aortic rings isolated from uPA$^{-/-}$ mice were incubated with pWPXL-based LV at 100 multiplicity of infection in EBM-2 medium for 24 h. The rings were then embedded in Matrigel and layered with EBM-2 medium containing VEGF. On day 8, sequences of images were taken in various z sections at 3.3-μm intervals to visualize GFP-expressing cells within the vessel, which were then subjected to three-dimensional reconstitution using ImageJ software. A virtual three-dimensional image of the GFP-expressing cells within the aortic ring is shown. Color-coded sequential position of each z-section is indicated on the scale on the *left panel*. *B*, RT PCR analysis of the total RNA samples isolated from the empty-, WT-uPA- and ΔK-uPA-LV-transfected aortic rings. *C*, sprouting from the aortae of uPA$^{-/-}$ mice transfected with the empty-, WT-uPA-, and ΔK-uPA- LVs. Sprouting was stimulated with VEGF (100 ng/ml) in EBM-2 medium. Representative images from five-six experiments under each of the conditions are shown. *D*, *bar graph* showing mean ± S.E. area (*top*) or length (*bottom*) of sprouts from aortae of WT or uPA$^{-/-}$ mice after stimulation with VEGF. **, $p < 0.001$ for value uPA LV *versus* value for KO con LV; *, $p < 0.001$ for value uPA LV *versus* value for KO DK-uPA LV; #, $p < 0.01$ for value con LV *versus* value for KO DK-uPA LV.

binding to HHEX. uPA variants were immobilized onto the wells of a 96-well plate. Immobilized uPAs were then incubated with nuclear extracts from 293 HEK cells transfected with HHEX-FLAG/pcDNA3 plasmid, which encodes full-length HHEX possessing a FLAG tag at the C terminus. WT-scuPA and ΔGFD-scuPA bound HHEX, in contrast to ATF, which lacks the proteolytic domain, and low molecular weight-uPA or ΔK-scuPA, which lacks the kringle (Fig. 8*D*). This result indicates that both the kringle and the C-terminal proteolytic domain are necessary for binding to HHEX.

To determine whether uPA induces expression of VEGFR1 and VEGFR2 by interfering with the repressor function of HHEX, we used the K562 cell line. K562 cells express low levels of endogenous uPA, and they express both VEGFR1 and VEGFR2, which can be suppressed by ectopic expression of HHEX (51). K562 cells were co-transfected with the HHEX- and/or uPA-encoding vectors alone or in combination, and VEGFR1 and VEGFR2 mRNA levels were measured. The results shown in Table 1 demonstrate that overexpression of HHEX suppresses both VEGFR1 and VEGFR2 mRNA levels.

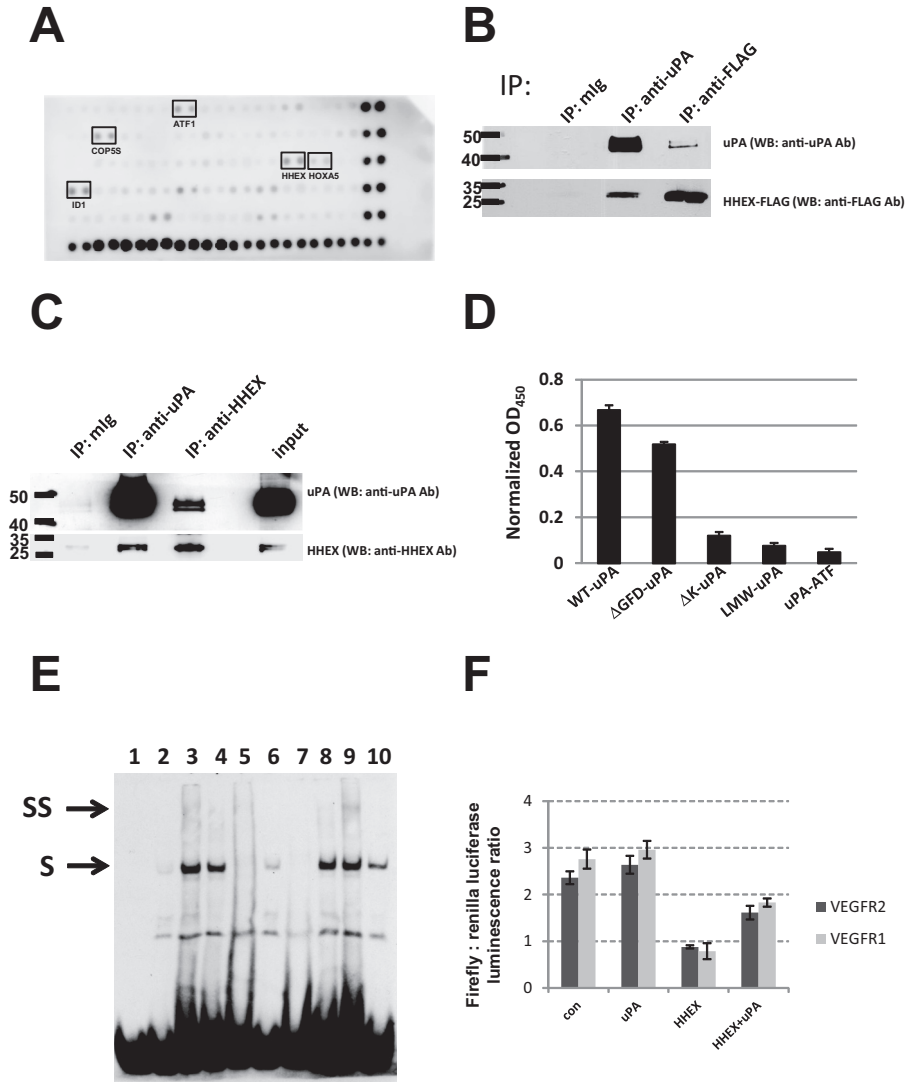

FIGURE 8. **Functional consequences of uPA binding to HHEX.** *A*, TranSignal Transcription factor Protein Array. Array Membranes (Panomics, Version I) spotted in duplicate with proteins expressed from full-length transcription factor cDNAs were incubated with scuPA (10 nM) for 2 h. Bound scuPA was detected with rabbit anti-uPA polyclonal antibodies, HRP-conjugated secondary goat anti-rabbit antibodies, and chemiluminescence substrate. *B*, co-immunoprecipitation (*co-IP*) of uPA and HHEX from 293HEK cells ectopically expressing HHEX-FLAG and uPA. HEK 293 cells were transfected with HHEX-FLAG in pcDNA3.1 and uPA/pcDNA3.1 vectors. Two days later, cells were harvested, and nuclear extracts were prepared using the NucBuster protein extraction kit (Novagen). uPA or HHEX was immunoprecipitated using mouse monoclonal anti-uPA or anti-FLAG antibodies immobilized on agarose beads. Normal mouse Ig immobilized on agarose beads was used as the negative control. Immune complexes were analyzed by Western blot (*WB*) using anti-uPA rabbit polyclonal antibodies and HRP-conjugated anti-FLAG mouse monoclonal antibodies. *C*, co-immunoprecipitation of uPA and HHEX from the nuclear extracts of human scuPA-treated human LMVECs. uPA and HHEX were co-immunoprecipitated from the nuclear extracts using mouse monoclonal anti-uPA and anti-HHEX antibodies, respectively. Normal mouse Ig immobilized on agarose beads was used as the negative control. Immune complexes were analyzed by Western blot using anti-uPA rabbit polyclonal antibodies and anti-HHEX rabbit polyclonal antibody. *D*, binding of HHEX to recombinant uPA variants. Recombinant uPA variants (33 nM in PBS) or BSA (1%) as the negative control were immobilized in 96-well plates in triplicate and incubated with nuclear extract from HEK293 cells transfected with pcDNA 3.1/HHEX-FLAG. Bound HHEX-FLAG was detected using an anti-HHEX polyclonal antibody/HRP-anti-rabbit antibody sandwich ELISA. Optical density was read at 450 nm (OD_{450}). *y* axes denote *normalized* OD_{450} obtained by subtracting the OD_{450} measured in BSA-coated wells from the OD_{450} measured in wells coated with uPA variants. *E*, uPA inhibits binding of HHEX to the target DNA sequence. HEK 293 cells were transfected with HHEX-FLAG in pcDNA3.1. Two days later, cells were harvested, and nuclear extracts were prepared. EMSA reactions were performed using biotinylated double-stranded HHEX specific oligonucleotides and corresponding unlabeled oligonucleotide. *1*, no nuclear extracts (*NE*); *2*, + NE in presence of 50× excess unlabeled HHEX-specific oligonucleotide; *3*, + NE alone; *4*, + NE in the presence of BSA; *5*, + scuPA (500 ng); *6*, + NE + scuPA (500 ng); *7*, + scuPA in the presence of anti-uPA antibody; *8*, + NE + mouse IgG; *9*, + NE + anti-FLAG mouse monoclonal antibody; 10, + NE in the presence of irrelevant unlabeled oligonucleotides. *S*, probe shift caused by HHEX overexpression. *SS*. probe supershift caused by HHEX-bound anti-FLAG antibody. *F*, VEGFR1 and VEGFR2 promoter luciferase reporter assay. Human VEGFR1 or VEGFR2 promoter-driven luciferase reporter pGL3 (51) vectors were co-transfected in EA.hy926 cells with uPA- and HHEX-encoding pcDNA3.1 vectors alone or in combination. Luciferase activity was measured at 24 h using a Dual Luciferase Reporter assay kit (Promega). Outcomes were normalized to the activity of co-transfected renilla luciferase-encoding pRL-CMV vector (Promega).

Ectopic expression of uPA alone did not significantly change VEGFR1 or VEGFR2 expression, providing further evidence that uPA does not directly affect transcription of the VEGFR1 and VEGFR2 promoters. However, co-expression of uPA together with HHEX reversed HHEX-mediated repression of VEGFR1 and VEGFR2. These data suggest that binding of uPA to HHEX inhibits binding of the transcription factor to its target DNA sequence. To examine this possibility in more detail, we performed an EMSA using vegfr2 promoter-derived double-stranded oligonucleotide that contained a HHEX consensus region (see

TABLE 1

***Vegfr-1*, and *Vegfr-2* mRNA levels in K562 cells 48 hr after co-transfection with pMUG1 (empty vector), pMUG1-Myc-PRH, pSIH (empty vector), or pSIH-uPA**

Levels of mRNA were determined by quantitative reverse transcriptase-PCR using specific primers and compared to GAPDH mRNA. Values are shown as -fold change over control values obtained (means and S.E.) in a sample co-transfected with pMUG1 (empty vector) and pSIH (empty vector) ($n = 3$).

	vegfr-1		*vegfr-2*		*uPA*		*PRH*	
Expression vector(s)	Mean -fold change	S.E.	Mean -fold change	S.E.	Mean -fold change	S.E.	Mean -fold change	S.E.
pmug1-empty +pSIH3-empty	1		1		1		1	
pmug1-PRH +pSIH3-empty	0.759[a]	0.011	0.623[b]	0.07	0.710	0.21	728.09	299.74
pmug1-empty +pSIH3-uPA	1.499	0.122	1.569	0.19	549.227	524, 01	3.35	0.946
pmug1-PRH +pSIH3-uPA	2.331	1.13	1.414	0.62	183.469	69.21	181.95	30.34

[a] $p < 0.005$ relative to control (pmug1-empty+pSIH-empty).
[b] $p < 0.005$ relative to control (pmug1-empty+pSIH-empty).

"Experimental Procedures"). The data show that WT scuPA did not bind directly to the HHEX DNA consensus sequence, but it did inhibit binding of HHEX to its DNA target site (Fig. 8*E*).

These hypotheses were further supported by the results of the VEGFR1 and VEGFR2 promoter luciferase reporter assay. Expression of HHEX resulted in a 3.49- and 2.68-fold repression of VEGFR1 and VEGFR2 promoter activities, respectively, whereas co-expression of HHEX with uPA partially but significantly reversed inhibition of VEGFR1 and VEGFR2 promoter activity by HHEX (Fig. 8*F*). These results provide additional support for the hypothesis that binding uPA to HHEX leads to de-repression of the VEGFR1 and VEGFR2 promoters.

Discussion

VEGF and uPA play prominent roles in angiogenesis (59, 66). $VEGF_{165}$ induces endothelial cell motility, invasion, and proliferation by binding to specific receptors, VEGFR1 (Flt-1) and VEGFR2 (KDR) (59). Binding of VEGF to these receptors up-regulates the expression of uPA and generates plasmin that converts catalytically inactive scuPA into enzymatically active tcuPA (67). tcuPA proteolyzes extracellular matrices and induces intracellular signal transduction through autocrine and paracrine pathways that promote endothelial cell proliferation and migration (for review, see Ref. 66). In this manuscript we describe an additional mechanism by which uPA promotes angiogenesis, *i.e.* via transcriptional up-regulation of VEGFR1 and VEGFR2 expression.

Our findings show that proliferation of human and mouse microvascular endothelial cells in response to VEGF-A requires the presence of uPA in the nucleus where it binds to the transcription factor HHEX. Binding of uPA of HHEX interferes with transcriptional repression of the *vegfr1* and *vegfr2* promoters leading to up-regulation of receptor expression.

Nuclear translocation of uPA in endothelial cells does not require uPAR, as both full-length uPA and a variant lacking the uPAR binding GFD are both able to translocate to cell nuclei (37) (Fig. 4*C*) and up-regulate both VEGF receptors (Fig. 6*B*). Rather, translocation of uPA to the nucleus and up-regulation of expression of VEGF receptors depends on its kringle domain (37) (Figs. 4*B* and 6*A*). We previously reported that nuclear translocation of uPA is mediated by nucleolin (37), a nucleocytoplasmic shuttle protein that transports diverse proteins from the cytoplasm to the nucleus (68). Nucleolin is located on the external plasma membrane of angiogenic endothelial lining tumor vessels but not on neighboring endothelium lining non-proliferating host vessels (69), but how its appearance on cell surfaces is regulated is unknown. Blockade of cell surface nucleolin with a specific pseudopeptide reduces tumor progression in mouse models of cancer (70, 71). Therefore, the preferential translocation of nucleolin onto the surface of angiogenic endothelial cells may promote nuclear translocation of uPA and lead to de-repression of VEGFRs expression.

To find the intranuclear target for uPA responsible for its pro-angiogenic activity, we profiled uPA-binding transcription factors using a transcription factor protein-protein microarray. We found that uPA binds transcription factor HHEX, also referred to as proline-rich homeodomain protein (PRH) transcription factor, which has been identified by us previously as a transcriptional repressor of the *vegfr1* and *vegfr2* promoters (51).

We chose one of the potential HHEX DNA sequences derived from the *vegfr2* promoter to help elucidate the mechanism by which uPA modulates the DNA binding capacity of HHEX. Our data show that uPA does not bind directly to this dsDNA oligonucleotide. Rather, uPA binds to HHEX (Fig. 8, *A–C*), inhibiting its capacity to dock onto its target DNA sequence (Fig. 8*E*). Our data also demonstrate that overexpression of HHEX/PRH reduces VEGFR1 and VEGFR2 mRNA expression and that co-expression of HHEX and uPA prevents repression of VEGFR1 and VEGFR2 by HHEX/PRH. Therefore, our data suggest that in quiescent endothelial cells HHEX represses expression of VEGF receptors. In contrast, overexpression of uPA in response to VEGF (67) or other mediators released by tumors or surrounding stroma (31, 72) as well as release of uPA by tumor or stromal cells (73, 74) may "sensitize" endothelial cells to pro-angiogenic stimuli through uPA-mediated de-repression of VEGFRs promoters, thereby promoting angiogenesis even in the absence of a significant change in VEGF expression *per se*.

uPA might also regulate angiogenesis by binding to other transcription factors that activate or repress additional genes. For example, we recently reported that uPA promotes survival of pancreatic cancer cells in part by binding to the homeobox transcription factor HOXA5 leading to down-regulation of p53 expression (38). Sustained expression of HOXA5 leads to down-regulation of many pro-angiogenic genes including *vegfr2*, *ephrin A1*, *Hif1α*, and *cox-2* (39). Additional studies are needed to determine whether binding of uPA to HOXA5 and

other homeobox transcription factors in endothelial cells promotes angiogenesis during physiological and pathological angiogenesis by inducing an angiogenic switch through coordinate up-regulation and/or down-regulation of genes involved in endothelial cell proliferation, adhesion, and migration. These data also suggest that targeting nuclear transport of uPA through its kringle or the motif that mediates its binding to transcription factors might provide novel means to control aberrant angiogenesis with minimal impact on healthy vasculature.

Author Contributions—V. S. contributed to conception of the research, designed and performed the research, analyzed the data, and wrote the paper. P.-S. J. contributed to conception of the research, designed the research, and analyzed the data. S. V. Z., T. L., I. B., K. B., E. S., K. H., and R. K. performed the research and analyzed the data. Y. V. P. coordinated the research and analyzed data. V. A. T. contributed to conception of the research and coordinated the research. D. B. C. contributed to conception of the research and wrote the paper. All authors reviewed the results and approved the final version of the manuscript.

Acknowledgments—We thank Yasmina Bdeir, Anastasia Makarova, and Maria Boldyreva for technical assistance, Xinyu Zhao and the Microscopy Core Facility at the Department of Cell and Developmental Biology, University of Pennsylvania Perelman School of Medicine for assistance with the Imaging procedures, Dr. Serge Yarovoi for providing the muPA/pMT/BiP plasmid, Dr. Alexander Y. Shevelev for providing pSIH-hUPA plasmid, and Dr. V. P. Krymskaya for critical reading of the manuscript.

References

1. Geudens, I., and Gerhardt, H. (2011) Coordinating cell behaviour during blood vessel formation. *Development* **138,** 4569–4583
2. Eilken, H. M., and Adams, R. H. (2010) Dynamics of endothelial cell behavior in sprouting angiogenesis. *Curr. Opin. Cell Biol.* **22,** 617–625
3. Chung, A. S., and Ferrara, N. (2011) Developmental and pathological angiogenesis. *Annu. Rev. Cell Dev. Biol.* **27,** 563–584
4. Hanahan, D., and Folkman, J. (1996) Patterns and emerging mechanisms of the angiogenic switch during tumorigenesis. *Cell* **86,** 353–364
5. Eilken, H. M., and Adams, R. H. (2010) Turning on the angiogenic microswitch. *Nat. Med.* **16,** 853–854
6. Devy, L., Blacher, S., Grignet-Debrus, C., Bajou, K., Masson, V., Gerard, R. D., Gils, A., Carmeliet, G., Carmeliet, P., Declerck, P. J., Nöel, A., and Foirdart, J.-M. (2002) The pro- or antiangiogenic effect of plasminogen activator inhibitor 1 is dose dependent. *FASEB J.* **16,** 147–154
7. Montuori, N., and Ragno, P. (2014) Role of uPA/uPAR in the modulation of angiogenesis. *Chem. Immunol. Allergy* **99,** 105–122
8. Traktuev, D. O., Tsokolaeva, Z. I., Shevelev, A. A., Talitskiy, K. A., Stepanova, V. V., Johnstone, B. H., Rahmat-Zade, T. M., Kapustin, A. N., Tkachuk, V. A., March, K. L., and Parfyonova, Y. V. (2007) Urokinase gene transfer augments angiogenesis in ischemic skeletal and myocardial muscle. *Mol. Ther.* **15,** 1939–1946
9. Boudreau, N., Andrews, C., Srebrow, A., Ravanpay, A., and Cheresh, D. A. (1997) Induction of the angiogenic phenotype by Hox D3. *J. Cell Biol* **139,** 257–264
10. Pepper, M. S., Sappino, A. P., Stöcklin, R., Montesano, R., Orci, L., and Vassalli, J. D. (1993) Upregulation of urokinase receptor expression on migrating endothelial cells. *J. Cell Biol* **122,** 673–684
11. Mazar, A. P., Henkin, J., and Goldfarb, R. H. (1999) The urokinase plasminogen activator system in cancer: implications for tumor angiogenesis and metastasis. *Angiogenesis* **3,** 15–32
12. Cubellis, M. V., Nolli, M. L., Cassani, G., and Blasi, F. (1986) Binding of single chain prourokinase to the urokinase receptor of human U937 cells. *J. Biol. Chem.* **261,** 15819–15822
13. Blasi, F. (1988) Surface receptors for urokinase plasminogen activator. *Fibrinolysis* **2,** 73–84
14. Nykjaer, A., Kjøller, L., Cohen, R. L., Lawrence, D. A., Garni-Wagner, B. A., Todd, R. F., 3rd, van Zonnenfeld, A.-J., Gliemann, J., and Andreasen, P. A. (1994) Regions involved in binding of urokinase-type-1 inhibitor complex and pro-urokinase to the endocytic α2-macroglobulin receptor/low density lipoprotein receptor-related protein: evidence that the urokinase receptor protects pro-urokinase against binding to the endocytic receptor. *J. Biol. Chem.* **269,** 25668–25676
15. Pluskota, E., Soloviev, D. A., Bdeir, K., Cines, D. B., and Plow, E. F. (2004) Integrin αMβ2 orchestrates and accelerates plasminogen activation and fibrinolysis by neutrophils. *J. Biol. Chem.* **279,** 18063–18072
16. Kwak, S. H., Mitra, S., Bdeir, K., Strassheim, D., Park, J. S., Kim, J. Y., Idell, S., Cines, D., and Abraham, E. (2005) The kringle domain of urokinase-type plasminogen activator potentiates LPS-induced neutrophil activation through interaction with αVβ3 integrins. *J. Leukoc. Biol.* **78,** 937–945
17. Tarui, T., Akakura, N., Majumdar, M., Andronicos, N., Takagi, J., Mazar, A. P., Bdeir, K., Kuo, A., Yarovoi, S. V., Cines, D. B., and Takada, Y. (2006) Direct interaction of the kringle domain of urokinase-type plasminogen activator (uPA) and integrin αvβ3 induces signal transduction and enhances plasminogen activation. *Thromb. Haemost.* **95,** 524–534
18. Peltz, S. W., Hardt, T. A., and Mangel, W. F. (1982) Positive regulation of activation of plasminogen by urokinase: differences in Km for (glutamic acid)-plasminogen and lysine-plasminogen and effect of certain α, omega-amino acids. *Biochemistry* **21,** 2798–2804
19. Miles, L. A., Greengard, J. S., and Griffin, J. H. (1983) A comparison of the abilities of plasma kallikrein, β-Factor XIIa, Factor XIa and urokinase to activate plasminogen. *Thromb. Res.* **29,** 407–417
20. Matrisian, L. M. (1992) The matrix-degrading metalloproteinases. *Bioessays* **14,** 455–463
21. Okumura, Y., Sato, H., Seiki, M., and Kido, H. (1997) Proteolytic activation of the precursor of membrane type 1 matrix metalloproteinase by human plasmin: a possible cell surface activator. *FEBS Lett.* **402,** 181–184
22. Makowski, G. S., and Ramsby, M. L. (1998) Binding of latent matrix metalloproteinase 9 to fibrin: activation via a plasmin-dependent pathway. *Inflammation* **22,** 287–305
23. Baramova, E. N., Bajou, K., Remacle, A., L'Hoir, C., Krell, H. W., Weidle, U. H., Noel, A., and Foidart, J. M. (1997) Involvement of PA/plasmin system in the processing of pro-MMP-9 and in the second step of pro-MMP-2 activation. *FEBS Lett.* **405,** 157–162
24. Estreicher, A., Müllhauser, J., Carpentier, J.-L., Orci, L., and Vassalli, J.-D. (1990) The receptor for urokinase type plasminogen activator polarizes expression of the protease to the leading edge of migrating monocytes and promotes degradation of enzyme inhibitor complexes. *J. Cell Biol.* **111,** 783–792
25. Alexander, R. A., Prager, G. W., Mihaly-Bison, J., Uhrin, P., Sunzenauer, S., Binder, B. R., Schütz, G. J., Freissmuth, M., and Breuss, J. M. (2012) VEGF-induced endothelial cell migration requires urokinase receptor (uPAR)-dependent integrin redistribution. *Cardiovasc. Res.* **94,** 125–135
26. Prager, G. W., Breuss, J. M., Steurer, S., Olcaydu, D., Mihaly, J., Brunner, P. M., Stockinger, H., and Binder, B. R. (2004) Vascular endothelial growth factor receptor-2-induced initial endothelial cell migration depends on the presence of the urokinase receptor. *Circ. Res.* **94,** 1562–1570
27. Matsuno, H., Kozawa, O., Yoshimi, N., Akamatsu, S., Hara, A., Mori, H., Okada, K., Ueshima, S., Matsuo, O., and Uematsu, T. (2002) Lack of α2-antiplasmin promotes pulmonary heart failure via overrelease of VEGF after acute myocardial infarction. *Blood* **100,** 2487–2493
28. Ferrara, N. (2010) Binding to the extracellular matrix and proteolytic processing: two key mechanisms regulating vascular endothelial growth factor action. *Mol. Biol. Cell* **21,** 687–690
29. Park, J. E., Keller, G. A., and Ferrara, N. (1993) The vascular endothelial growth factor (VEGF) isoforms: differential deposition into the subepithelial extracellular matrix and bioactivity of extracellular matrix-bound VEGF. *Mol. Biol. Cell* **4,** 1317–1326
30. Saksela, O., and Rifkin, D. B. (1990) Release of basic fibroblast growth factor-heparan sulfate complexes from endothelial cells by plasminogen

activator-mediated proteolytic activity. *J. Cell Biol.* **110,** 767–775
31. Koolwijk, P., van Erck, M. G., de Vree, W. J., Vermeer, M. A., Weich, H. A., Hanemaaijer, R., and van Hinsbergh, V. W. (1996) Cooperative effect of TNFα, bFGF, and VEGF on the formation of tubular structures of human microvascular endothelial cells in a fibrin matrix: role of urokinase activity. *J. Cell Biol* **132,** 1177–1188
32. Plouët, J., Moro, F., Bertagnolli, S., Coldeboeuf, N., Mazarguil, H., Clamens, S., and Bayard, F. (1997) Extracellular cleavage of the vascular endothelial growth factor 189-amino acid form by urokinase is required for its mitogenic effect. *J. Biol. Chem.* **272,** 13390–13396
33. Heymans, S., Luttun, A., Nuyens, D., Theilmeier, G., Creemers, E., Moons, L., Dyspersin, G. D., Cleutjens, J. P., Shipley, M., Angellilo, A., Levi, M., Nübe, O., Baker, A., Keshet, E., Lupu, F., Herbert, J. M., Smits, J. F., Shapiro, S. D., Baes, M., Borgers, M., Collen, D., Daemen, M. J., and Carmeliet, P. (1999) Inhibition of plasminogen activators or matrix metalloproteinases prevents cardiac rupture but impairs therapeutic angiogenesis and causes cardiac failure. *Nat. Med.* **5,** 1135–1142
34. Behzadian, M. A., Windsor, L. J., Ghaly, N., Liou, G., Tsai, N. T., and Caldwell, R. B. (2003) VEGF-induced paracellular permeability in cultured endothelial cells involves urokinase and its receptor. *FASEB J.* **17,** 752–754
35. Prager, G. W., Mihaly, J., Brunner, P. M., Koshelnick, Y., Hoyer-Hansen, G., and Binder, B. R. (2009) Urokinase mediates endothelial cell survival via induction of the X-linked inhibitor of apoptosis protein. *Blood* **113,** 1383–1390
36. Makarova, A. M., Lebedeva, T. V., Nassar, T., Higazi, A. A., Xue, J., Carinato, M. E., Bdeir, K., Cines, D. B., and Stepanova, V. (2011) Urokinase-type plasminogen activator (uPA) induces pulmonary microvascular endothelial permeability through low density lipoprotein receptor-related protein (LRP)-dependent activation of endothelial nitric-oxide synthase. *J. Biol. Chem.* **286,** 23044–23053
37. Stepanova, V., Lebedeva, T., Kuo, A., Yarovoi, S., Tkachuk, S., Zaitsev, S., Bdeir, K., Dumler, I., Marks, M. S., Parfyonova, Y., Tkachuk, V. A., Higazi, A. A., and Cines, D. B. (2008) Nuclear translocation of urokinase-type plasminogen activator. *Blood* **112,** 100–110
38. Asuthkar, S., Stepanova, V., Lebedeva, T., Holterman, A. L., Estes, N., Cines, D. B., Rao, J. S., and Gondi, C. S. (2013) Multifunctional roles of urokinase plasminogen activator (uPA) in cancer stemness and chemoresistance of pancreatic cancer. *Mol. Biol. Cell* **24,** 2620–2632
39. Rhoads, K., Arderiu, G., Charboneau, A., Hansen, S. L., Hoffman, W., and Boudreau, N. (2005) A role for Hox A5 in regulating angiogenesis and vascular patterning. *Lymphat. Res. Biol.* **3,** 240–252
40. Chen, Y., and Gorski, D. H. (2008) Regulation of angiogenesis through a microRNA (miR-130a) that down-regulates antiangiogenic homeobox genes GAX and HOXA5. *Blood* **111,** 1217–1226
41. Kapustin, A., Stepanova, V., Aniol, N., Cines, D. B., Poliakov, A., Yarovoi, S., Lebedeva, T., Wait, R., Ryzhakov, G., Parfyonova, Y., Gursky, Y., Yanagisawa, H., Minashkin, M., Beabealashvilli, R., Vorotnikov, A., Bobik, A., and Tkachuk, V. (2012) Fibulin-5 binds urokinase-type plasminogen activator and mediates urokinase-stimulated β1-integrin-dependent cell migration. *Biochem. J.* **443,** 491–503
42. Bdeir, K., Kuo, A., Sachais, B. S., Rux, A. H., Bdeir, Y., Mazar, A., Higazi, A. A., and Cines, D. B. (2003) The kringle stabilizes urokinase binding to the urokinase receptor. *Blood* **102,** 3600–3608
43. Sobczak, M., Dargatz, J., and Chrzanowska-Wodnicka, M. (2010) Isolation and culture of pulmonary endothelial cells from neonatal mice. *J. Vis. Exp.* **46,** 2316
44. Dzhoyashvili, N. A., Efimenko, A. Y., Kochegura, T. N., Kalinina, N. I., Koptelova, N. V., Sukhareva, O. Y., Shestakova, M. V., Akchurin, R. S., Tkachuk, V. A., and Parfyonova, Y. V. (2014) Disturbed angiogenic activity of adipose-derived stromal cells obtained from patients with coronary artery disease and diabetes mellitus type 2. *J. Transl. Med.* **12,** 337
45. Efimenko, A., Dzhoyashvili, N., Kalinina, N., Kochegura, T., Akchurin, R., Tkachuk, V., and Parfyonova, Y. (2014) Adipose-derived mesenchymal stromal cells from aged patients with coronary artery disease keep mesenchymal stromal cell properties but exhibit characteristics of aging and have impaired angiogenic potential. *Stem Cells Transl. Med.* **3,** 32–41
46. Rubina, K., Kalinina, N., Potekhina, A., Efimenko, A., Semina, E., Poliakov, A., Wilkinson, D. G., Parfyonova, Y., and Tkachuk, V. (2007) T-cadherin suppresses angiogenesis in vivo by inhibiting migration of endothelial cells. *Angiogenesis* **10,** 183–195
47. Semina, E. V., Rubina, K. A., Sysoeva, V. Y, Makarevich, P. I., Parfyonova, Y. V., and Tkachuk, V. A. (2015) The role of urokinase in vascular cell migration and in regulation of growth and branching of capillaries. *Tsitologiia* **57,** 689–698
48. Larusch, G. A., Merkulova, A., Mahdi, F., Shariat-Madar, Z., Sitrin, R. G., Cines, D. B., and Schmaier, A. H. (2013) Domain 2 of uPAR regulates single-chain urokinase-mediated angiogenesis through β1-integrin and VEGFR2. *Am. J. Physiol. Heart Circ. Physiol.* **305,** H305–H320
49. Stepanova, V., Mukhina, S., Köhler, E., Resink, T. J., Erne, P., and Tkachuk, V. A. (1999) Urokinase plasminogen activator induces human smooth muscle cell migration and proliferation via distinct receptor-dependent and proteolysis-dependent mechanisms. *Mol. Cell. Biochem.* **195,** 199–206
50. Dumler, I., Stepanova, V., Jerke, U., Mayboroda, O. A., Vogel, F., Bouvet, P., Tkachuk, V., Haller, H., and Gulba, D. C. (1999) Urokinase-induced mitogenesis is mediated by casein kinase 2 and nucleolin. *Curr. Biol.* **9,** 1468–1476
51. Noy, P., Williams, H., Sawasdichai, A., Gaston, K., and Jayaraman, P. S. (2010) PRH/Hhex controls cell survival through coordinate transcriptional regulation of vascular endothelial growth factor signaling. *Mol. Cell. Biol.* **30,** 2120–2134
52. Deindl, E., Ziegelhöffer, T., Kanse, S. M., Fernandez, B., Neubauer, E., Carmeliet, P., Preissner, K. T., and Schaper, W. (2003) Receptor-independent role of the urokinase-type plasminogen activator during arteriogenesis. *FASEB J.* **17,** 1174–1176
53. Cao, G., Abraham, V., and DeLisser, H. M. (2014) Isolation of endothelial cells from mouse lung. *Curr. Protoc. Toxicol.* **61,** 24
54. Gupta, K., Kshirsagar, S., Li, W., Gui, L., Ramakrishnan, S., Gupta, P., Law, P. Y., and Hebbel, R. P. (1999) VEGF prevents apoptosis of human microvascular endothelial cells via opposing effects on MAPK/ERK and SAPK/JNK signaling. *Exp. Cell Res* **247,** 495–504
55. Kanno, S., Oda, N., Abe, M., Terai, Y., Ito, M., Shitara, K., Tabayashi, K., Shibuya, M., and Sato, Y. (2000) Roles of two VEGF receptors, Flt-1 and KDR, in the signal transduction of VEGF effects in human vascular endothelial cells. *Oncogene* **19,** 2138–2146
56. Gélinas, D. S., Bernatchez, P. N., Rollin, S., Bazan, N. G., and Sirois, M. G. (2002) Immediate and delayed VEGF-mediated NO synthesis in endothelial cells: role of PI3K, PKC and PLC pathways. *Br. J. Pharmacol.* **137,** 1021–1030
57. Yoshioka, K., Yoshida, K., Cui, H., Wakayama, T., Takuwa, N., Okamoto, Y., Du, W., Qi, X., Asanuma, K., Sugihara, K., Aki, S., Miyazawa, H., Biswas, K., Nagakura, C., Ueno, M., Iseki, S., Schwartz, R. J., Okamoto, H., Sasaki, T., Matsui, O., Asano, M., Adams, R. H., Takakura, N., and Takuwa, Y. (2012) Endothelial PI3K-C2α, a class II PI3K, has an essential role in angiogenesis and vascular barrier function. *Nat. Med.* **18,** 1560–1569
58. Dellinger, M. T., and Brekken, R. A. (2011) Phosphorylation of Akt and ERK1/2 is required for VEGF-A/VEGFR2-induced proliferation and migration of lymphatic endothelium. *PloS ONE* **6,** e28947
59. Olsson, A. K., Dimberg, A., Kreuger, J., and Claesson-Welsh, L. (2006) VEGF receptor signalling: in control of vascular function. *Nat. Rev. Mol. Cell Biol.* **7,** 359–371
60. Ruvinsky, I., and Meyuhas, O. (2006) Ribosomal protein S6 phosphorylation: from protein synthesis to cell size. *Trends Biochem. Sci.* **31,** 342–348
61. Salerno, G., Verde, P., Nolli, M. L., Corti, A., Szöts, H., Meo, T., Johnson, J., Bullock, S., Cassani, G., and Blasi, F. (1984) Monoclonal antibodies to human urokinase identify the single-chain pro-urokinase precursor. *Proc. Natl. Acad. Sci. U.S.A.* **81,** 110–114
62. Wun, T. C., Ossowski, L., and Reich, E. (1982) A proenzyme form of human urokinase. *J. Biol. Chem.* **257,** 7262–7268
63. Nassar, T., Yarovoi, S., Fanne, R. A., Akkawi, S., Jammal, M., Allen, T. C., Idell, S., Cines, D. B., and Higazi, A. A. (2010) Regulation of airway contractility by plasminogen activators through *N*-methyl-D-aspartate receptor-1. *Am. J. Respir. Cell Mol. Biol.* **43,** 703–711
64. Kasai, S., Arimura, H., Nishida, M., and Suyama, T. (1985) Proteolytic

cleavage of single-chain pro-urokinase induces conformational change which follows activation of the zymogen and reduction of its high affinity for fibrin. *J. Biol. Chem.* **260,** 12377–12381
65. Hofer, E., and Schweighofer, B. (2007) Signal transduction induced in endothelial cells by growth factor receptors involved in angiogenesis. *Thromb. Haemost.* **97,** 355–363
66. Breuss, J. M., and Uhrin, P. (2012) VEGF-initiated angiogenesis and the uPA/uPAR system. *Cell Adh. Migr.* **6,** 535–615
67. Prager, G. W., Breuss, J. M., Steurer, S., Mihaly, J., and Binder, B. R. (2004) Vascular endothelial growth factor (VEGF) induces rapid prourokinase (pro-uPA) activation on the surface of endothelial cells. *Blood* **103,** 955–962
68. Tuteja, R., and Tuteja, N. (1998) Nucleolin: a multifunctional major nucleolar phosphoprotein. *Crit. Rev. Biochem. Mol. Biol.* **33,** 407–436
69. Christian, S., Pilch, J., Akerman, M. E., Porkka, K., Laakkonen, P., and Ruoslahti, E. (2003) Nucleolin expressed at the cell surface is a marker of endothelial cells in angiogenic blood vessels. *J. Cell Biol* **163,** 871–878
70. Krust, B., El Khoury, D., Soundaramourty, C., Nondier, I., and Hovanessian, A. G. (2011) Suppression of tumorigenicity of rhabdoid tumor derived G401 cells by the multivalent HB-19 pseudopeptide that targets surface nucleolin. *Biochimie* **93,** 426–433
71. El Khoury, D., Destouches, D., Lengagne, R., Krust, B., Hamma-Kourbali, Y., Garcette, M., Niro, S., Kato, M., Briand, J. P., Courty, J., Hovanessian, A. G., and Prévost-Blondel, A. (2010) Targeting surface nucleolin with a multivalent pseudopeptide delays development of spontaneous melanoma in RET transgenic mice. *BMC Cancer* **10,** 325
72. Tobar, N., Villar, V., and Santibanez, J. F. (2010) ROS-NFκB mediates TGF-β1-induced expression of urokinase-type plasminogen activator, matrix metalloproteinase-9 and cell invasion. *Mol. Cell. Biochem.* **340,** 195–202
73. Buø, L., Bjørnland, K., Karlsrud, T. S., Kvale, D., Kjønniksen, I., Fodstad, O., Brandtzaeg, P., Johansen, H. T., and Aasen, A. O. (1994) Expression and release of plasminogen activators, their inhibitors and receptor by human tumor cell lines. *Anticancer Res.* **14,** 2445–2451
74. Nielsen, B. S., Sehested, M., Duun, S., Rank, F., Timshel, S., Rygaard, J., Johnsen, M., and Danø, K. (2001) Urokinase plasminogen activator is localized in stromal cells in ductal breast cancer. *Lab. Invest.* **81,** 1485–1501